Chemie der Erde - Geochemistry - Interdisciplinary Journal for Chemical Problems of the Geosciences and Geoecology xxx (xxxx) xxx

Contents lists available at ScienceDirect

Geochemistry

journal homepage: www.elsevier.com/locate/chemer

Genesis of the Late Archean granitoids of the northern part of the Dharwar foreland (Dharwar Craton), south India – Insights from field, crystal size distribution, thermobarometry, microgeochemical and bulk-rock geochemical studies

Chandan K. Boraiaha [a,b,*], Annappa G. Ugarkar [b], Jayant K. Padhi [a], Rashmi Chandan [a,b], Mallappa V. Kallapur [b]

[a] Ore Research & Exploration Group, Department of Geology, Central University of Kerala, Kasaragod -671 320, Kerala, India
[b] Department of Studies in Geology, Karnatak University, Pavatenagar, Dharwad – 580 003, Karnataka, India

ARTICLE INFO

Handling Editor: Orhan Karsli

Keywords:
Dharwad granitoids
Dharwar Foreland
CSD
Magma chamber processes
Crustal evolution

ABSTRACT

An intrusive granitoid pluton into TTG-Dharwar Supergroup greenstone sequence is being reported for the first time from the Dharwar Foreland region. Based on field and petrographic characteristics, these granitoids are classified as - quartz-monzodiorites and granites. Occasional mafic bodies of dioritic-granodioritic composition with size ranging from small microgranular magmatic enclaves to bodies of several centimeters are common in these granitoids.

The granitoids are devoid of any crystal-plastic fabric as well as high-strain characteristics. The textural (CSD) studies indicate that the quartz-monzodiorites are derived from magma mixing whereas the granites are derived from equilibrium crystallization of the magma derived from the reworking of quartz-monzodiorites. The P-T estimates indicate that the quartz-monzodiorites were crystallized at higher temperature (>950 °C) and pressure (3.09–4.36 kbar) conditions in a reducing environment at mid-crustal levels. However, the granites indicate lower temperature (<750 °C) and pressure (0.89–1.88 kbar) conditions of crystallization in an oxidizing environment at shallow-crustal levels. The bulk rock chemical characteristics indicate that the quartz-monzodiorites were derived from the melt generated by the mixing of two melts - a melt derived from the differentiation of sanukitoids senso lato (s.l.) and a melt derived from the partial melting of TTG. On the other hand, reworking of the hot crystallizing quartz-monzodiorite due to its rapid upliftment to shallow crustal levels resulted in a decompression melting which gave rise to granitic melts.

The relative age of the Dharwad granitoids is estimated to be ~2580–2560 Ma and unlike the other older granitoids (> 2.61 Ga) reported from the northern part of the Shimoga greenstone belt, the studied granitoids marks the final stage of cratonization in the Foreland region.

1. Introduction

Bulk-rock geochemical studies combined with high-precision isotopic data of mafic-felsic magmatic rocks have been widely used in the last two decades to investigate the fundamental architecture, time-frame of crustal accretion and reworking as well as petrogenetic processes during Archean Martin et al. (2005); Smithies et al. (2005); Hawkesworth et al. (2010, 2013); Condie (2014); Chandan-Kumar and Ugarkar (2017); Dhuime et al. (2018); Jayananda et al. (2020, 2018, 2013). This is because in majority of the cases the magmatic rocks retain valuable information pertaining to the origin of their source magmas and its geodynamic emplacement. However, chances of losing these information or misinterpreting the available evidences are more, if the rocks have undergone significant post-magmatic alterations on a large scale and/or in cases where the rocks are completely recycled due to anatexis (Taylor et al., 1984; Davidson et al., 2007). This is evident in the fact that despite significant advances made in deciphering the timing and mechanisms of major Archean craton building processes, secular changes in the compositions of juvenile additions as well as the tectonic context of Archean continental growth are still topics of debate

* Corresponding author at: Ore Research & Exploration Group, Department of Geology, Central University of Kerala, Kasaragod-671 320, Kerala, India.
E-mail address: rcgeo85@icloud.com (C.K. Boraiaha).

https://doi.org/10.1016/j.chemer.2020.125688
Received 5 May 2020; Received in revised form 21 July 2020; Accepted 27 September 2020
Available online 18 October 2020

(Jayananda et al., 2020, and references therein).

To ensure there is no loss of primary data due to post-magmatic alteration and avoid the misinterpretation of bulk-rock geochemical and isotopic data, an integrated approach involving combination of field, mineralogical and textural compositions of common rock forming minerals, micro-geochemistry, bulk-rock geochemistry and isotopic data is proposed. The compositions and assemblages of common (meta) igneous rock forming minerals retain valuable information pertaining to the origin of the magmas, evolving physicochemical conditions of the melt during crystallization and the post-solidus modification of the resulting rock units (Helmy et al., 2004). Pressure and temperature (P-T) estimates of magmatic emplacement and the halogen contents in the

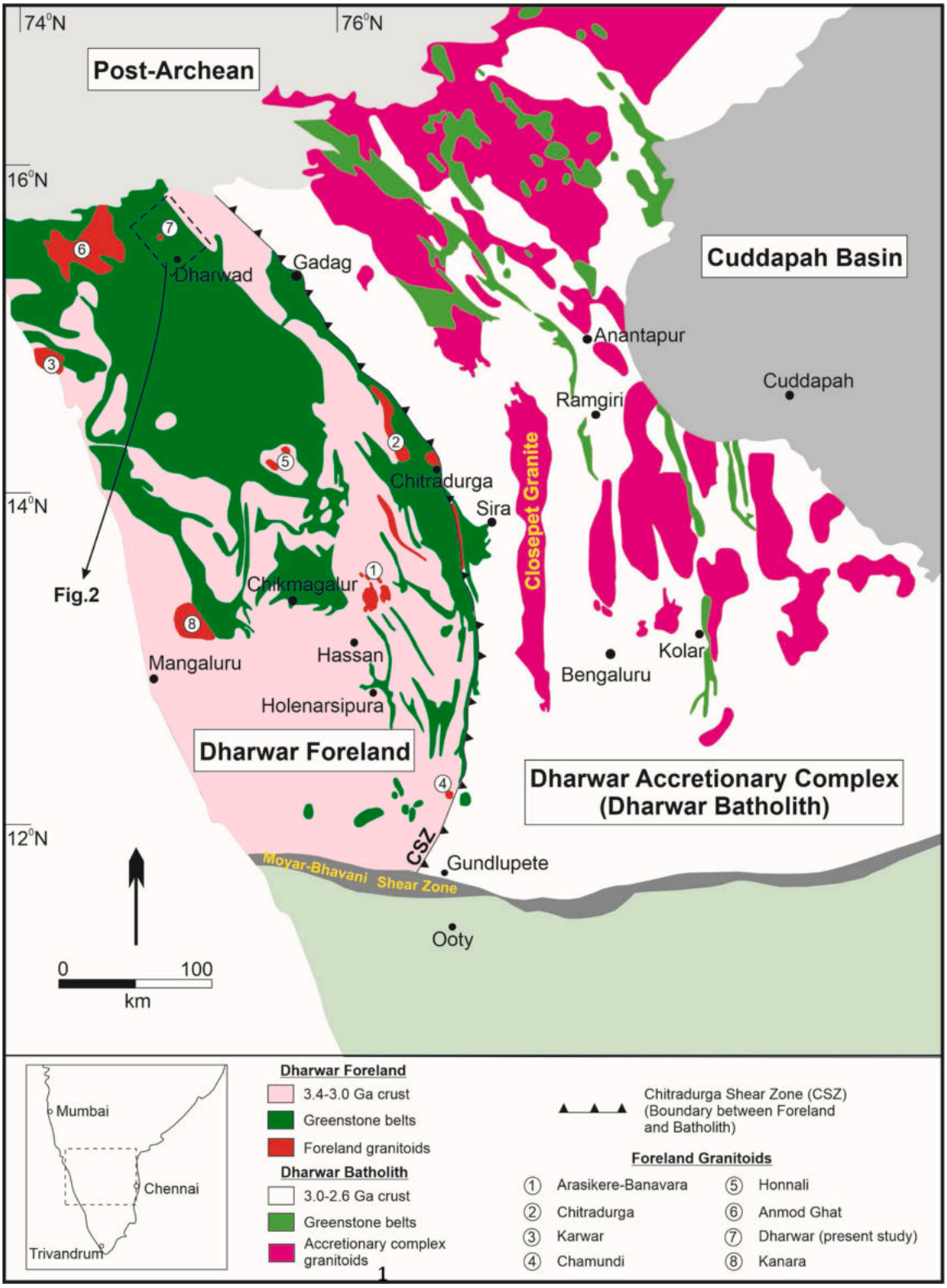

Fig. 1. Outline geological map of the Dharwar Craton, southern Peninsular India (modified after Chadwick et al., 2007 and Devaraju et al., 2009).

common rock-forming hydrous mineral phases (hornblende and biotite) plays a significant role in the investigations related to magmatic evolution and crustal growth processes (Putirka, 2008; Ridolfi et al., 2010; Selby and Nesbitt, 2000; Boomeri et al., 2010; Xianwu et al., 2009; Siahcheshm et al., 2012). Evaluating magmatic processes is fundamental to understand the petrogenesis of (meta)igneous rocks that were widely responsible in controlling the Archaean crustal architecture. A proper understanding of the textures and compositions of (meta)igneous rocks provides a wider window to investigate the magmatic processes. For instance, textural features of a magmatic rock directly depends on the rate of cooling and crystal nucleation, growth rate and residence time (Vernon, 2018). Further, quantitative textural analyses (i.e. crystal size, form and orientation) also helps in understanding the physical characteristics of magma crystallization (Higgins, 2006; Jerram and Higgins, 2007).

An attempt has been made in this paper to investigate the petrogenesis of the Late Archean granitoids and to link the genesis of these granitoids to the Late Archaean crustal evolution process in the Dharwar Foreland region. An integrated approach, involving the investigation of evidences obtained from the field, mineralogical, textural, microgeochemical and bulk-rock studies, is effectively utilized in this paper to achieve the objectives.

2. Geological framework

2.1. Regional geology

Following summary of the regional geology of the Dharwar foreland (also known as Western Dharwar Craton) is taken from Rogers (1988); Chadwick et al. (2000); Ramakrishnan and Vaidyanadhan (2010); Ramachandra (2016); Chandan-Kumar and Ugarkar (2017); Boraiaha et al. (2018); Jayananda et al. (2018); Devaraju et al. (2009, 2007). The foreland region (Fig.1) predominantly comprises of 3.363.2 Ga tonalite-trondhjemite-granodiorite (TTG) gneiss, which forms the basement for the two suites of supracrustal (greenstone) belts. The 3.58–3.23 Ga early-mid Archean supracrustal belts, engulfed within the TTG gneisses, form small enclaves towards the southern part of the Foreland region. On the other hand, the 2.9–2.6 Ga younger supracrustal belts are underlain by either the early-mid Archean supracrustal sequences or the basement TTG gneisses.

The early-mid Archean supracrustal belts (known as Sargur Group) consists predominantly of 3.35 Ga komatiite-basalt association (Jayananda et al., 2008), with occasional 3.29 Ga felsic volcanic rocks (Peucat et al., 1995) and inter-layered 3.58–3.23 Ga sediments (quartzite-pelite-carbonate-banded iron formations) (Nutman et al., 1992; Ramakrishnan et al., 1994). The overlying late Archean Dharwar Supergroup of rocks that are found in the 2.9–2.6 Ga younger supracrustal belts are divided into a lower Bababhudan and an upper Chitradurga Groups. The Bababhudan Group comprises of clasts-supported oligomict conglomerate, quartzite, voluminous mafic flows [2.9–2.8 Ga; (Kumar et al., 1996)], phyllite, felsic volcanic tuffs [2.72 Ga; (Trendall et al., 1997a, b)], and thick banded iron formations (BIFs). On the other hand, the Chitradurga Group has a matrix-supported polymict conglomerates at its base, which are successively overlain by 2.75-Ga mafic volcanics (Kumar et al., 1996), dominant greywackes-argillite containing carbonate beds, and 2.61-Ga felsic volcanics (Nutman et al., 1996) with BIFs at the top of the succession (Chadwick et al., 1981).

This older-younger supracrustal sequences are locally intruded by 2.61-Ga potassic plutons as a result of the reworking of its lower crust (Chadwick et al., 2007; Jayananda et al., 2006; Nutman et al., 1996; Taylor et al., 1984). Within the foreland region, metamorphic conditions in the supracrustal belts increase southward from greenschist to amphibolite facies.

2.2. Younger granitoids of Dharwar foreland

Few examples of younger granites (≤2.6 Ga) reported from the southern part of the foreland region are Arasikere-Banavara granite, Chitradurga granite, Karwar granite and Chamundi granite (Fig. 1) (Crawford, 1969; Venkatasubramanian and Naryanaswamy, 1974; Taylor et al., 1984; Rogers, 1988; Mohan et al., 2014). These younger granites (except Chamundi Granite) range in age from 2.6 to 2.5 Ga and they exhibit intrusive relationship with the basement TTGs. The Chamundi granite is reported to be much younger at 790 ± 60 Ma (Crawford, 1969). The granitoids in the north of the foreland region reported in this study are a new find and is being reported for the first time as per our knowledge. These granitoids are termed as *Dharwad Granitoids* in this study as they are found in the close vicinity to the Dharwad Town in Karnataka state (Fig. 2). These granitoids were discovered during the geological mapping program conducted in the northern part of the foreland region by (Ugarkar et al., 2012). The extensively studied younger granites in the southern part of the Dharwar foreland region are situated outside the supracrustal (greenstone) belts (Ramakrishnan and Vaidyanadhan, 2010), while the Dharwad granitoids of the present study occur within the Shimoga supracrustal belt and has discordant relationship with the litho units of the supracrustal belt. The detailed geology of Shimoga supracrustal belt is very well illustrated in the works of Harinadha Babu et al. (1981); Chadwick et al. (1988); Srinivasan and Naha (1993); Ugarkar et al. (2017); Boraiaha et al. (2018); Giri et al. (2019).

3. Dharwad Granitoids – an overview

3.1. Field characteristics

The Dharwad granitoids occur widely northwest of Dharwad city and it forms the mound at Agasanahalli village (Fig. 2). The granites are inferred to cut sharply across the planar fabric of the thick sequences of metasediments, especially metagreywackes and banded iron formations (BIF) of Shimoga supracrustal sequence. In general, the foliation and schistosity of the host metasediments strike NNW-SSE and the dip varies between 75 °E (occasionally west) and vertical. The BIF occurs interlayered with the metagreywackes and occasionally they are deformed. The Dharwad granitoids are fairly homogeneous, coarse- to medium-grained, dark to light grey varieties that grades into pink granite (Fig. 3a–c). Occasional mafic bodies of dioritic-granodioritic composition with size ranging from small microgranular magmatic enclaves (MME) to bodies of several centimeters are common in these granitoids (Fig. 3d). Based on the field characteristics and modal mineralogical investigations carried out in the field on the fresh outcrop surfaces (with a 10 cm × 10 cm grid), the Dharwad granitoids are classified as granodiorite, grey granite and pink granite (Fig. 4). The mesocratic granodiorite consists of abundant plagioclase and mafic mineral phases (pyroxenes and amphiboles) with subordinate quartz and potash feldspar while the leucocratic grey and pink granites are dominated by two-feldspars and quartz with decreasing mafic mineral abundances from grey to pink varieties. The mineralogy of the MMEs resemble the studied granodiorites. The MMEs contain predominantly plagioclase, amphiboles, quartz and alkali feldspars. They are relatively fine grained compared to the granodiorites. The studied granitoids are devoid of crystal-plastic fabric and are thus, undeformed (Hutton, 1988; Chadwick et al., 1996). They also lack large (>2 cm) feldspar phenocrysts that characterizes certain granitic types (e.g. Closepet granites; Jayananda et al., 1995) in the Dharwar Craton. Further, the studied granitoids, unlike their gneissic counterpart (which forms the basement for the supracrustal sequence and granitoids) lack sheared, folded, migmatitic and high-strain characteristics.

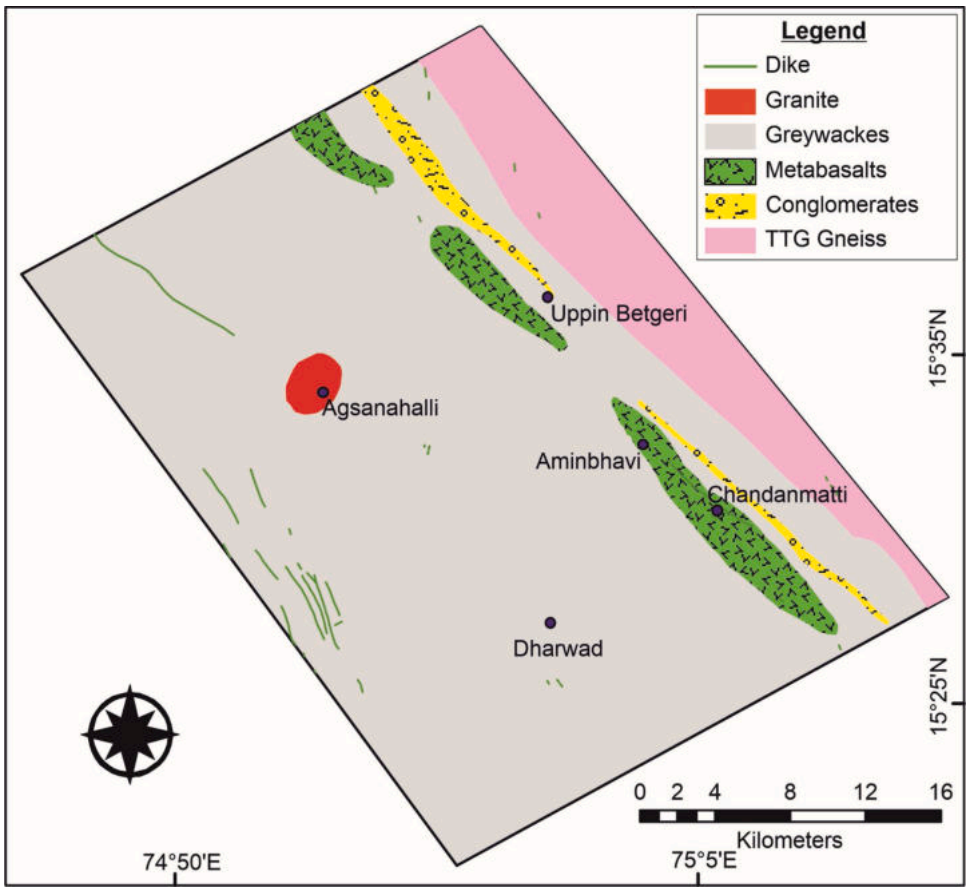

Fig. 2. Geological map of the northern part of the Shimoga greenstone belt in the Dharwar Foreland region (Ugarkar et al., 2017).

Fig. 3. Field photographs: (a) sub-circular outcrops of granitoids near Agasanahalli village; (b) medium-coarse grained granodiorite; (c) broken fresh sample of pink-granite; (d) magmatic enclaves within granitoids.

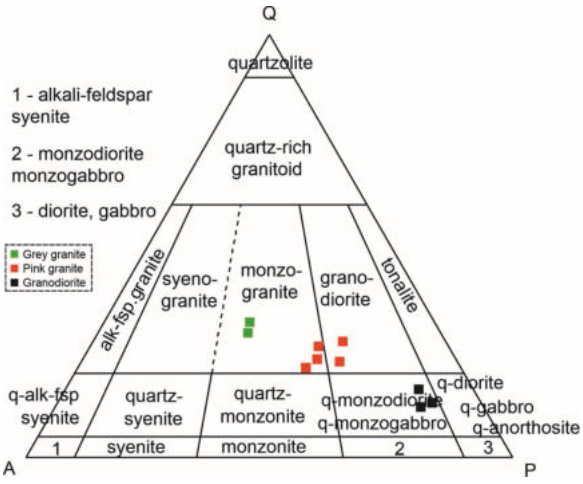

Fig. 4. QAP classification diagram of Dharwad granitoids (Streckeisen, 1974).

3.2. Mineralogical and textural characteristics

The studied granitoids occupy three different fields in the quartz-alkali feldspar-plagioclase (QAP) classification diagram of Streckeisen (1974) (Fig. 4). The mesocratic granodiorite samples occupy quartz monzodiorite-field, while leucocratic grey and pink granite samples occupy granite-field (Fig. 4; Table 1). Two of the grey granite samples occupy granodiorite-field due to the abundance of opaque-oxide phases in the studied sections. For the sake of convenience and owing to their petrographic characteristics, the studied granodiorites and granites (grey and pink) will be referred to as quart monzodiorites and granites respectively, in this study.

The quartz monzodiorites consists of plagioclase (~60%), amphibole (~20%), quartz (~10%), alkali felspar (~6%) and pyroxene (~4%) (Fig.4; Table 1). The plagioclase crystals are usually coarse grained (~5 mm) and forms phenocrysts that are embedded in the medium to fine grained ground mass that consists of amphibole, quartz, alkali-feldspar and pyroxene (Fig. 5a–c). The majority of the plagioclase crystals found in the studied quartz monzodiorite have cores with high calcium (Ca) content (labradorite to anorthite) and rims with moderate to high sodium content (albitic) as determined by Michael Levy method (Kerr, 1959). Orthoclase is the dominant alkali feldspar. Occasionally, orthoclase is perthitic, with exsolution strings and rods. Alteration of amphiboles and pyroxenes to chlorite are not uncommon. The predominating mafic phase present in the quartz monzodiorites is hornblende and a lesser clinopyroxene (5b-d). Occasional blebs of hornblende filling the fractures in clinopyroxene crystals indicates the sub-solidus origin of certain hornblende crystals (Otten, 1984). Post-emplacement alteration seems prominent which is indicated by the highly sassuritized plagioclase cores. Mantling of chloritized hornblende crystals over quartz, resorbed quartz grain boundaries and embayed quartz crystals (Fig. 5d,e) are some of the significant textural features that characterizes quartz-monzodiorite. Occasional quartz-feldspar inter-growth (granophyric texture) in the interstitial spaces between the plagioclase laths are observed. The accessory phases include titanomagnetite, ilmenite, apatite, zircon and epidote in the order of their abundance (Fig. 6a–e). The magnetite exhibit blocky euhedral crystal shape with occasional skeletal and boxy crystals containing inclusions of amphibole (Fig. 6d). Apatites are present as long needles (~1 mm) as well as euhedral prismatic stubby crystals (Fig. 6a) associated with the mafic phases such as hornblende and biotite.

The major mineralogy in the grey granites in decreasing order of abundance includes plagioclase (~33%), alkali felspar (~31%), quartz (~20%) and mafic mineral phases (~16%) (Fig. 4; Table 1). The plagioclase exhibit lath shaped crystals and vary in composition from labradorite to albite as determined by Michael Levy's method (Kerr, 1959). Microcline (with occasional orthoclase) is the dominant alkali feldspar. Most of the microcline are perthitic with exsolution lamellae and strings. The most abundant mafic mineral phase is hornblende (~12%) followed by a smaller proportion of biotite (~4%). Unlike quartz-monzodiorite, pyroxenes are absent in the grey granites. The grey granites often contain blebs of relatively smaller quartz crystals rimming the plagioclase and alkali feldspar crystals giving rise to granophyric texture (Fig. 7a,b). Mantling of biotite over amphibole is also a common feature (Fig. 7c). The accessory minerals include titanomagnetite, ilmenite, apatite, zircon and minor epidote (7d,e). Apatite often occurs as stubby euhedral crystals and rarely as long needles (~1 mm) (Fig. 7d) and are usually associated with the mafic silicate phases.

The pink granites mineralogically resemble their grey counterpart. The mineralogy of pink granites in decreasing order of abundance includes plagioclase (~36%), alkali feldspar (~31%), quartz (~27%) and mafic mineral phases (~12.94%) (Fig. 4; Table 1). Alkali felspars are commonly microcline (with or without minor orthoclase) and are almost equal in abundance as that of quartz (Fig. 8a–d). The intensity of perthite occurrence increases from almost negligible in quartz-monzodiorites to moderate in grey-granites to excessive in pink-granites. Plagioclase composition varies between labradorite and albite as determined by Michael Levy's method (Kerr, 1959). The pink granite predominantly exhibits graphic inter-growth texture. The myrmekitic inter-growth in the rims of plagioclase and alkali felspar crystals is a common feature. The granophyric texture becomes more pronounced in the pink granites. Occasionally, inter-growth of epidote and feldspar crystals are seen (Fig. 8c). The studied pink granites contain minor amount of mafic phases, the major mafic phase being the opaque iron oxides. The accessory phases include zircon and minor epidote.

4. Analytical methods

4.1. Crystal size distribution (CSD)

The Crystal Size Distribution (CSD) is a quantitative textural analysis tool which was first developed by Larson and Randolph (1971) to study industrial crystallization processes. The usage of the technique in petrology was developed by Marsh (1988); Cashman and Marsh (1988).

Table 1
Modal analyses of the granitoid varieties in the northern part of the Foreland region.

Sample ID	Quartz	K-feldspar	Plagioclase	Pyroxene	Amphibole	Biotite	Rock type
GD1	9.28	7.85	55	3.21	25	–	
GD2	13.07	7.69	49.23	–	29.23	–	Granodiorite
GD3	9.44	6.11	55	–	27.78	1.66	
GG1	18.75	20	43.75	–	16.25	1.25	
GG2	18.75	27.5	41.25	–	12.5	–	
GG3	18.57	22.85	38.57	–	20	–	Grey Granite
GG4	23.33	17.77	43.33	–	13.33	1.33	
GG5	22.94	22.94	41.17	–	12.94	–	
PG1	30	39.23	30.76	–	–	–	Pink Granite
PG2	31.42	38.57	30.42	–	–	–	

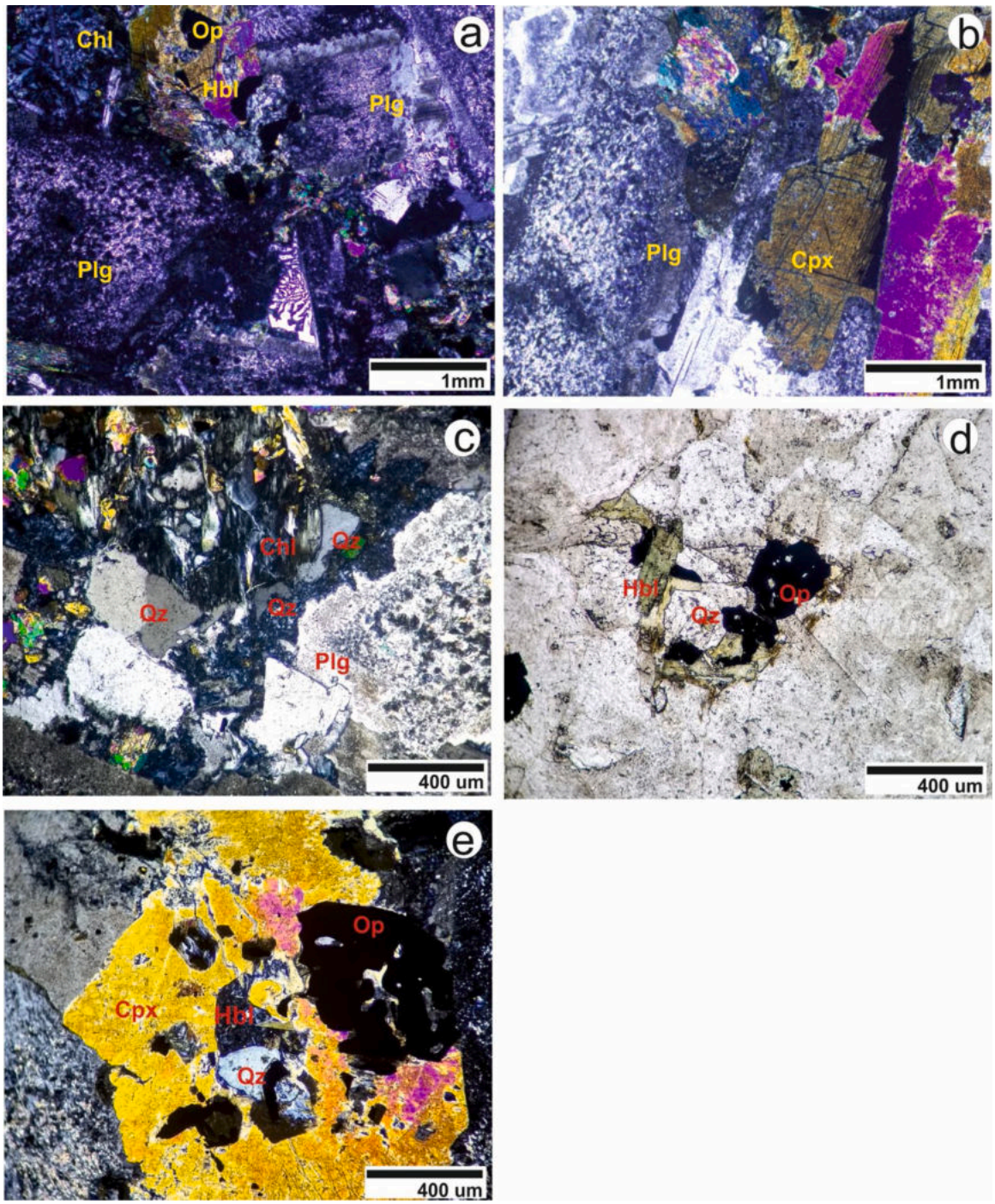

Fig. 5. Photomicrographs of quartz-monzodiorite (a) inter-growth texture exhibited by feldspar and amphibole; (b) lath shaped clinopyroxene crystals (c) resorption of quartz and plagioclase grain boundaries, also note the chloritized- hornblende growth along the resorbed boundaries; (d) mantling of hornblende and magnetite over quartz; (e) inclusion of quartz in hornblende, also note the embayments in quartz and hornblende 5within opaque oxides (magnetite).

The parameters used are the crystal sizes (maximum length, maximum width and area) plotted with their population density in a log-log scale. The curves hence produced indicate the nucleation and growth rates. Specific patterns also correspond to various igneous processes that resulted in the formation of the crystals and the enclosing rock as they are seen (Cashman and Marsh, 1988; Higgins, 2000, 2006; Chakraborti et al., 2017; Deb and Bhattacharyya, 2018). CSD was performed on plagioclase crystals of the three rock variants of Dharwad granitoids. The thin sections of the representative samples were studied in detail under the petrographic microscope (Olympus BX-53) available at Ore Research and Exploration Lab at Central University of Kerala, India. The photomicrographs of each field of view were taken with at least 30–50% overlap to produce a mosaic of the entire thin section. The plagioclase crystals in the photomicrographs were digitized using the Corel draw (X8) software and exported to black and white uncompressed tiff format (Fig. 9). The final image is then analyzed using the image analysis software called ImageJ. The scale of the image was input and analytical parameters were set to measure crystal length, width and area. However, these measured data represent only two-dimensional parameters, which need to be converted to three dimensions for crystal size distribution analysis. To convert this 2D data into 3D data, two hurdles need to be overcome namely (i) cut section effect and (ii) intersection

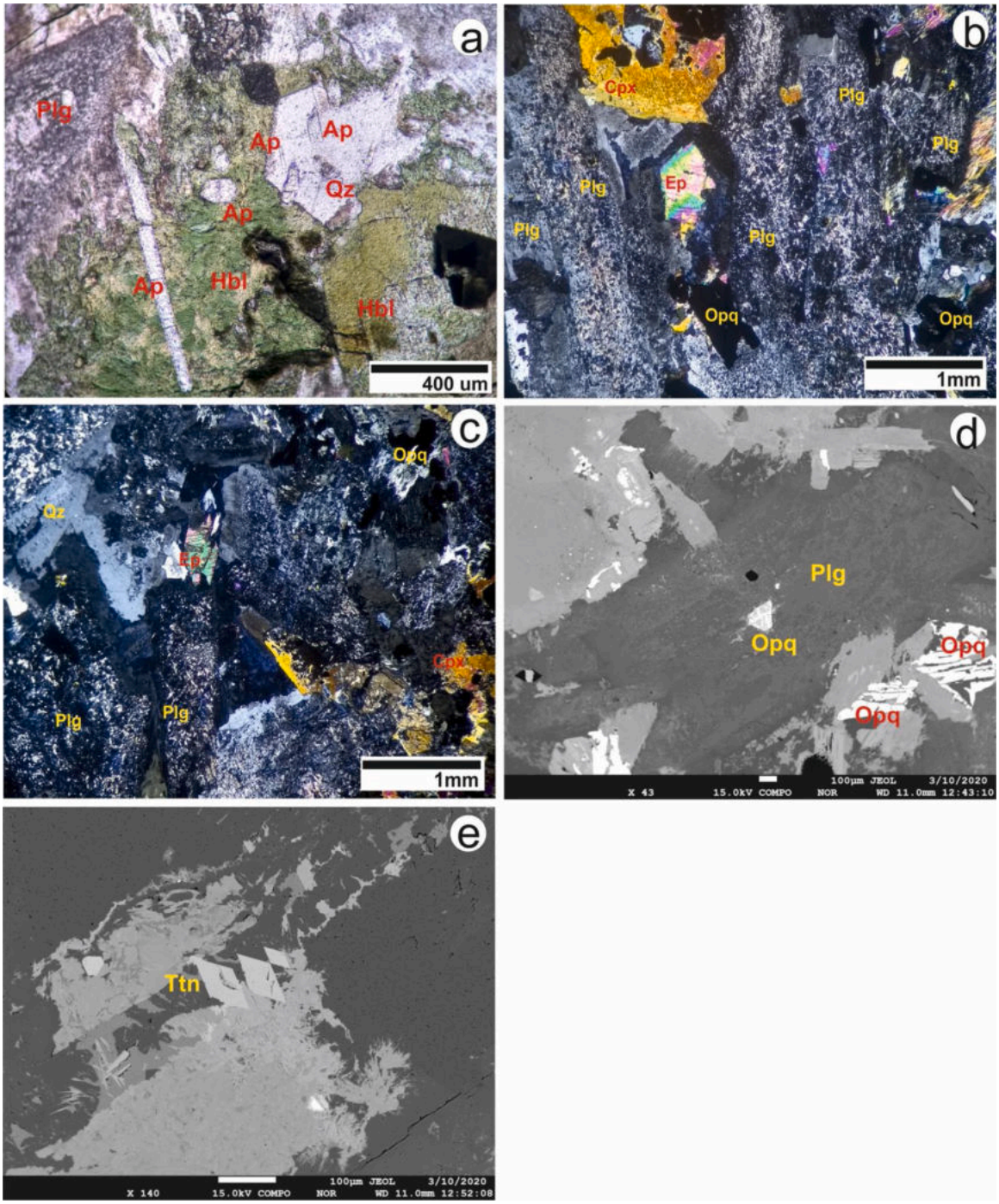

Fig. 6. Photomicrographs of quartz-monzodiorite (a) mixed morphologies of apatite; (b) and (c) euhedral epidote within the interstices between the plagioclase laths; (d) back-scattered image opaque-oxide inclusion exhibiting lamellar twinning (between magnetite and ilmenite) within plagioclase; (e) back- scattered image showing euhedral titanite crystals.

probability effect (Higgins, 2000). The thin section rarely cuts a crystal symmetrically or passes through the centre of each crystal. Hence, even if the crystals are of same size in the section, their three-dimensional attributes might be different. This uncertainty is known as cut section effect. Also, in a rock containing crystals of various sizes, the smaller crystals are less likely to be intersect by the thin section plane than the larger crystals, hence, in the thin section, the population density of the smaller crystals will be low. The program CSD Correction 1.6 (version 2018) (Higgins, 2000) was used in the study to rectify the errors that were generated due to the intersection probability and the cut section effects. Apart from the crystal size data, the software needs input data of average 3D crystal habit, roundness and sample foliation. The roundness and foliation data were measured by eye estimation. The value of degree of roundness of crystals ranges from 0 to 1 (with 0 being a rectangular and 1 an elliptical) and the foliation of rocks ranges 0–1 (0 for no foliation and 1 for strong foliation). The samples used in this study contained plagioclase crystals that are angular in shape and the rocks do not show any foliation, hence the values 0 and 0 were used for degree of roundness and foliation respectively. The 3D crystal aspect ratios were determined using the methodology followed by Higgins (2000). 3D crystal shapes (S : I : L; short axis : intermediate axis : long axis) are calculated as 1:2.6:3 for quartz monzodiorites, 1:3.94:5.88 for grey

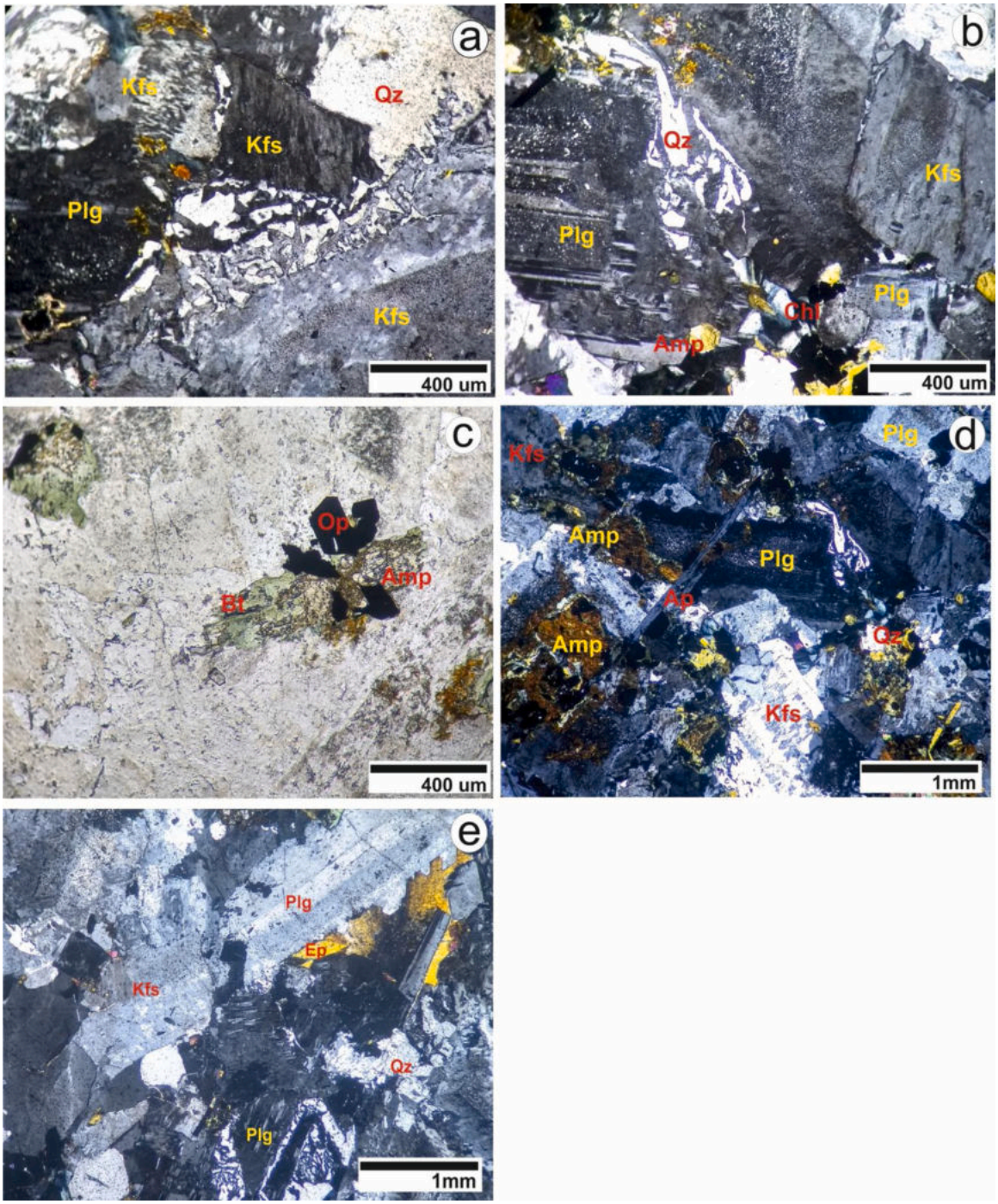

Fig. 7. Photomicrographs of grey-granites (a) inter-growth texture exhibited quartz and alkali-feldspar; (b) blebs of quartz at the rim of plagioclase crystal; (c) mantling of biotite over amphibole crystals; (d) acicular apatite crystals in grey granites; (e) euhedral epidote crystals within the interstices between plagioclase laths.

granites and 1:2:7.44 for pink granites.

4.2. Mineral chemistry and bulk-rock geochemistry

Mineral compositional mapping was performed using a JEOL JXA-8230 Superprobe, an Electron Probe MicroAnalyzer (EPMA), housed at the Advanced Facility for Microscopy and Microanalysis, Indian Institute of Science (IISc), Bangalore, India. Analyses were done using an accelerating voltage of 15 kV; beam current of 20 nA; and counting time of 10 s. Natural and synthetic silicates and oxides supplied by JEOL and ASTIMEX Standards Ltd., Canada were used for calibration. The data were reduced using the ZAF correction procedures supplied by JEOL.

Major oxides were analyzed by X-ray Fluorescence (XRF) technique at National Centre for Earth Science Studies (NCESS), Trivandrum, India. Pressed pellets were used respectively for major element analysis. The pellets were prepared by sprinkling finely powdered sample over boric acid binder filled in aluminum cups and pressing in a 40-ton hydraulic press for 30 s. Analyses were performed on a Bruker S4 Pioneer wavelength dispersive (WD) XRF instrument. The detection limit of major element was ~0.01% and analytical precision is always better than 1%. Precision for trace elements is estimated to be better than 5% on the basis of repeated analysis of reference rock standards (Kumar and Sreejith, 2016; Sorcar et al., 2019). The precision and accuracy of calibration curves and data reliability is available at http://cess.res.in/gr

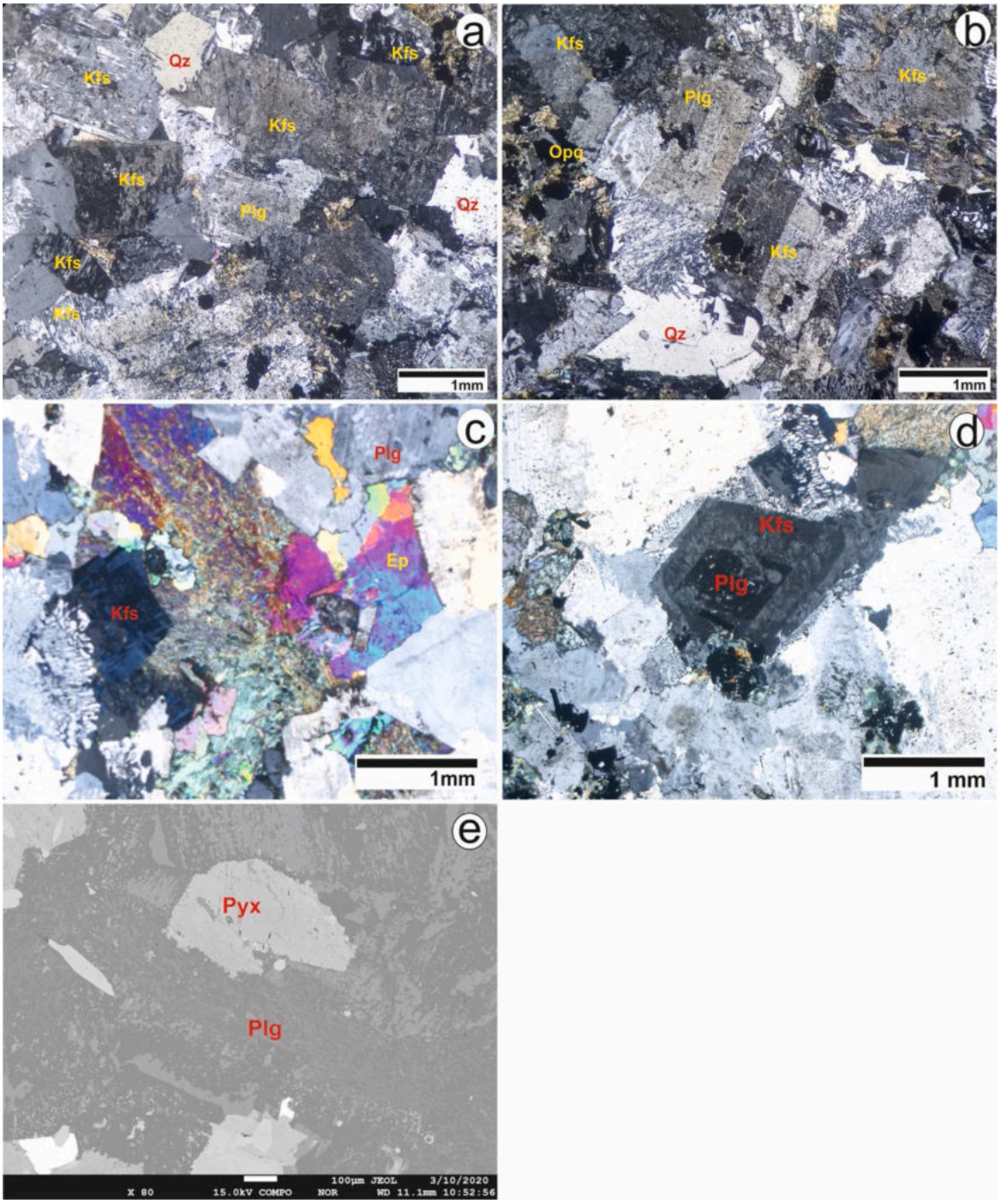

Fig. 8. Photomicrographs of pink-granites (a) perthitic K-feldspar associated with quartz and plagioclase; (b) orthoclase in association with opaque- oxides (magnetite-ilmenite), plagioclase and quartz; (c) epidote associated with k-feldspar, plagioclase and quartz; (d) zoned feldspar - growth of k-feldspar over the plagioclase crystals; (e) pyroxene within pink granite, note the anhedral resorbed boundary of the pyroxene crystal.

oups/crustal-processes-crpgroup/laborataries/xrf-lab-2.

Trace element concentration analyses were performed at Department of Earth Sciences in Indian Institute of Technology, Kanpur. Approximately 0.25 g of sampler powder was initially digested in pre-cleaned teflon beakers at 130 ± 5 °C using a 5 mL mixture of concentrated HF (2 parts), concentrated HCl (1 part) and concentrated HNO_3(1 part) for 48 h. The acid was then slowly evaporated at 80 ± 5 °C, and again the samples were redissolved in 4 mL of Aqua Regia acid (3 mL of concentrated HNO_3+ 1 mL of concentrated HCl). Aqua Regia was fluxed for 24 h. Further, the samples were dried and re-dissolved in 5% HNO_3. The acid digestion steps were only repeated when digestion was incomplete. Trace element concentrations were determined at ~200 ppm total dissolved solid solutions. Three procedural blanks, reference material SBC-1 (shale) and AGV-2 (andesite) rock standard from US Geological Survey (USGS) were also digested following the same procedures. The blanks were analyzed to quantify the total procedural blank, whereas AGV-2 was analyzed as an unknown to assess the data quality. SBC-1 was diluted to seven appropriate concentrations to construct the calibration curve, and trace element concentrations were determined based on the SBC-1 calibration curve. Since rock-matrix matched reference materials were unavailable, all the samples and standards were spiked by ~5 ppb In solution and In was used as an

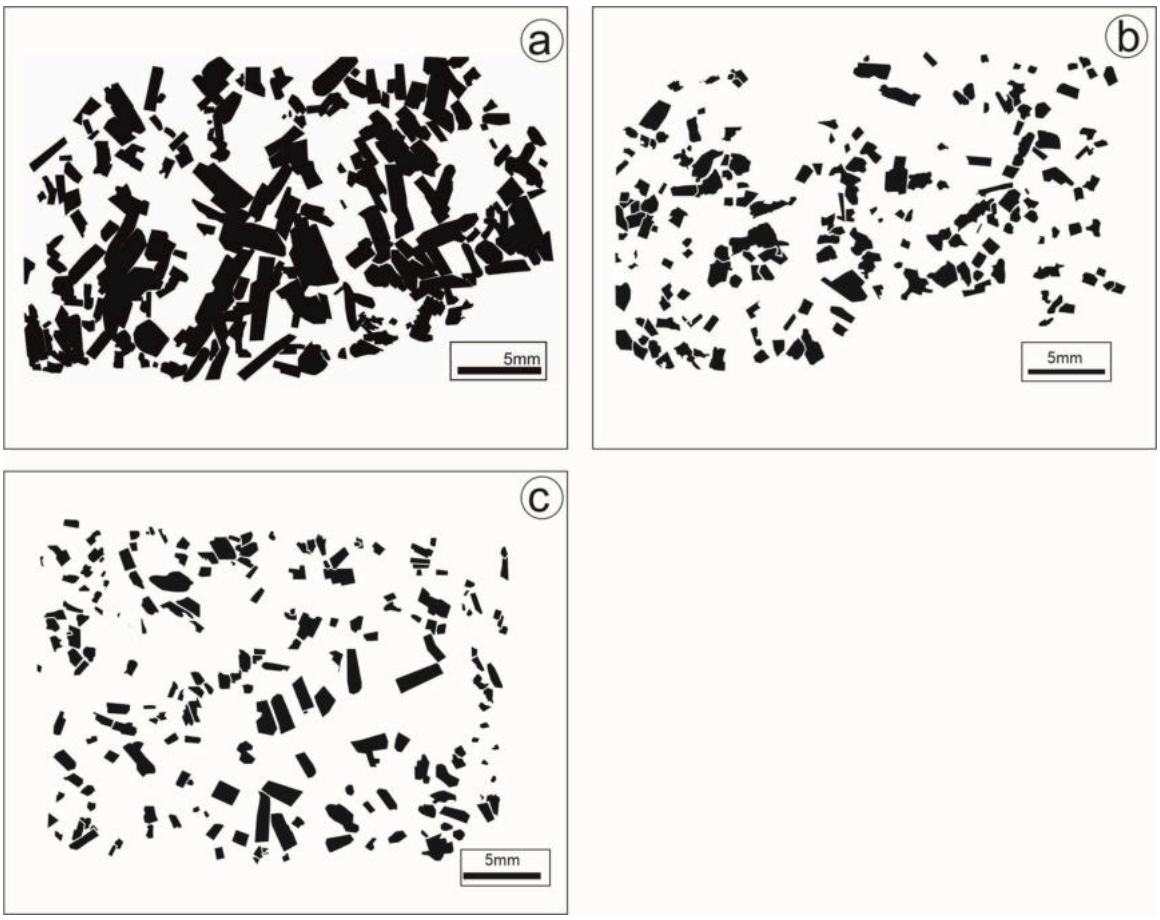

Fig. 9. Traced shapes of plagioclase crystals in (a) quartz-monzodiorite; (b) grey-granite; and (c) pink granite.

internal standard. The instrument was run both in standard and He kinetic energy discrimination mode to optimize the separation of measured isotopes from interfering polyatomic interferences. The final concentrations were blank – corrected using the average procedural blank concentrations and matrix effect was corrected by In normalization. Average blank corrections were less than 10% for most of the elements. The measured trace element concentration of AGV-2 agrees well with the USGS certified values.

Table 2
Chemical composition (wt%) and structural formulae of plagioclase (GD - Quartz monzodiorite; GG - Grey granite; PG - pink granite).

Sample	1st gen					2nd gen									
	GD1			GD2		GD1		GG1		GG2		PG1		PG2	
	Core Av.(3)	Rim Av.(10)	Rim* Av.(2)	Core Av.(2)	Rim Av.(7)	Core Av.(3)	Rim Av.(7)	Core Av.(5)	Rim Av.(3)	Core Av.(2)	Rim Av.(6)	Core Av.(3)	Rim Av.(6)	Core Av.(5)	Rim Av.(5)
SiO_2	54.89	56.66	65.68	45.06	59.63	61.83	63.06	65.54	65.55	68.03	68.45	65.25	63.5	66.45	66.74
Al_2O_3	28.6	26.74	21.9	26.5	25.18	24.03	23.01	21.33	21.44	20.3	20.19	21.66	22.43	20.37	20.32
FeO	0.48	0.45	0.11	3.42	0.28	0.18	0.25	0.21	0.15	0.01	0.01	0.25	0.47	0.06	0.04
CaO	10.63	9.22	2.97	17.48	6.7	3.91	4.19	2	2.35	0.84	0.5	1.37	1.62	0.81	0.84
Na_2O	5.29	6.12	8.55	2.42	7.32	8.71	8.84	10.03	9.67	11.4	11.65	10.15	9.48	11.17	11.18
K_2O	0.34	0.38	0.76	0.11	0.75	0.93	0.68	0.47	0.89	0.07	0.06	0.87	1.51	0.24	0.22
Si	61.65	63.65	72.37	52.93	66.5	69.06	69.67	72.32	72.09	73.81	74.06	72.27	71.09	73.39	73.5
Al	37.86	35.4	28.44	36.68	33.16	31.64	29.98	27.75	27.8	25.96	25.75	28.28	29.64	26.52	26.37
Fe	0.45	0.42	0.1	3.36	0.26	0.17	0.23	0.2	0.14	0	0.01	0.23	0.45	0.05	0.04
Ca	12.79	11.09	3.5	21.99	8.05	4.69	4.96	2.36	2.77	0.98	0.58	1.62	1.94	0.96	0.99
Na	11.68	13.53	18.52	5.59	16.03	19.14	19.21	21.77	20.93	24.34	24.79	22.12	20.84	24.27	24.23
K	0.48	0.54	1.07	0.17	1.06	1.32	0.96	0.66	1.25	0.09	0.08	1.23	2.18	0.34	0.32
An	51	44	15	79	32	19	20	10	11	4	2	7	8	4	4
Ab	47	54	80	20	64	76	76	88	84	96	97	89	83	95	95
Or	2	2	5	1	4	5	4	3	5	0	0	5	9	1	1
Fe/Al	1.19	1.2	0.37	9.15	0.76	0.52	0.78	0.007	0.005	0.0002	0.0004	0.01	0.01	0.002	0.002

Rim* - Overgrowth of albitic rim with high Ab_{80}.

5. Results

5.1. Mineral chemistry

The micro-probe analyses of plagioclase, K-feldspar, amphibole, pyroxene and accessory phases such as ilmenite, magnetite and epidote are given in Table 2–7.

5.1.1. Plagioclase

Plagioclase is a dominant constituent in the Dharwad granitoids and the mineral chemistry of different generations is summarized in Table 2. First generation plagioclase crystals shows a wide variation in composition from labradorite to anorthite. The overall composition of the first generation plagioclase shows Anorthite (An) rich cores ($An_{52–98}$) than any of the other plagioclase types in the studied Dharwad granitoids. At rims, the plagioclase are more albitic (Ab) with Ab_{80-83}. The first generation plagioclase has negligible orthoclase (Or) content and they display normal to oscillatory zoning.

The second generation plagioclase crystals are characterized by anhedral to subhedral (rarely, euhedral) phenocrysts, complex twinning and reverse to oscillatory zoning. Generally, the second generation crystals have oligoclase to albitic core ($An_{12–2}$) surrounded by a andesine to albitic ($An_{23–4}$) rim. Exsolution of K-feldspar blebs within the plagioclase resulting in antiperthites occur occasionally in the studied grey granites. One of the antiperthitic crystal analyzed for its mineral chemistry consist of euhedral K-feldspar blebs of $Or_{97}Ab_3$ to $Or_{99}Ab_1$ occurring along twin boundaries of host plagioclase with An_4Ab_{96} to An_3Ab_{97}. Occasionally, growth of K-feldspar crystals mantling the second generation plagioclase feldspar crystals are seen (Fig. 8).

5.1.2. Potash feldspar

Microcline is the dominating potash feldspar in the Dharwad granites. Perthites are common and their concentration increases from grey to pink granites. Generally, the potash feldspars range between $Or_{94}Ab_6$ to $Or_{99}Ab_1$ (Table 3). Analysis of perthite shows that the albite and orthoclase (microcline) phases are at spots 96–100% pure with values for albite ranging between $An_2Ab_{66}Or_{32}$ and Ab_{100} and for orthoclase (microcline) between $Or_{62}An_1Ab_{38}$ to $Or_{96}An_1Ab_3$.

5.1.3. Amphibole

Amphibole is a dominating mafic mineral phase in the Dharwad granitoids. Structural formulae calculations are on the basis of 23 atoms of oxygen (O) (Table 4). All the analyzed amphibole grains are

Table 3
Chemical composition (wt%) and structural formulae of perthitic K-feldspar (GG - Grey granite; PG - Pink granite).

Sample	GG1		PG2	
	Kfs Av.(8)	Ab* (Av).2	Kfs Av.(9)	Ab* Av.(11)
SiO_2	64.89	70.4	66.23	84.8
Al_2O_3	18.53	18.88	17.84	8.37
FeO	0.03	0.05	0.08	0.1
CaO	0.01	0.43	0.19	0.37
Na_2O	0.2	10.88	2.56	4.1
K_2O	16.87	0.14	12.19	0.99
Si	74.74	75.8	74.48	88.73
Al	25.16	23.98	22.89	11
Fe	0.03	0.05	0.08	0.09
Ca	0.01	0.5	0.22	0.44
Na	0.45	23.07	5.53	8.99
K	24.78	0.2	16.84	1.43
An	0	2	1	12
Ab	2	97	25	79
Or	98	1	74	9

Ab* - Exsolved blebs of albite within K-feldspar.

Table 4
Chemical composition (wt%) and structural formulae of Amphibole (GD - Quartz monzodiorite; GG - Grey granite).

Sample	GD-A1		GG-A2	
	Core	Rim	Core	Rim
SiO_2	35.97	46.84	43.52	45.55
TiO_2	5.36	1.16	1.1	0.51
Al_2O_3	12.31	5.1	6.22	5.45
FeO	24.68	22.35	26.76	24.79
MnO	0.13	0.3	0.5	0.56
MgO	7.95	9.13	6.22	7.59
CaO	0.05	10	9.75	9.66
Na_2O	0.15	0.73	2.06	1.05
K_2O	9.03	0.53	0.94	0.84
Si	5.37	7.24	6.75	7.17
Ti	0.6	0.13	0.13	0.06
Al	2.17	0.93	1.14	1.01
Fe^{2+}	3.08	2.89	2.43	3.23
Mn^{2+}	0.02	0.04	0.07	0.07
Mg	1.77	2.1	1.44	1.78
Ca	0.01	1.66	1.62	1.63
Na	0.04	0.22	0.62	0.32
K	1.72	0.1	0.19	0.17
T (°C)	972	638	720	640

Table 5
Chemical composition (wt%) and structural formulae of Amphibole (Amp) and Pyroxene (Pyx) in pink granite).

	Amp Av. (10)
SiO_2	31.3
TiO_2	26.471
Al_2O_3	8.65
FeO	1.288
MnO	0.029
MgO	0.022
CaO	28.832
Na_2O	0.006
Si	5.025
Ti	3.196
Al	1.636
Fe^{2+}	0.172
Mn^{2+}	0.003
Mg	0.004
Ca	4.96
Na	0.002
T (°C)	1080
	Pyx Av. (16)
SiO_2	51.14
TiO_2	0.39
Al_2O_3	1.02
FeO	14.45
MnO	0.49
MgO	11.19
CaO	19.78
Na_2O	0.16
Wo	42
En	33
Fs	25
Q	1.94
J	0.02
T (°C)	1135

Table 6
Chemical composition (wt%) of accessory phases (ilmenite and magnetite).

	Ilmenite								Magnetite					
Spots	1	2	3	5	6	7	8	9	1	2	3	4	5	6
SiO_2	–	0.05	–	–	0.01	–	0.03	–	0.208	0.065	0.089	0.06	0.102	0.074
TiO_2	50.69	50.36	50.33	49.6	50.15	50.31	49.68	50.03	11.68	4.15	4.80	6.06	7.35	6.79
Al_2O_3	0.04	0.02	–	–	–	–	0.01	0.03	0.104	–	0.012	0.028	0.029	0.002
FeO	48.76	49.19	48.18	48.83	48.74	47.86	48	48.64	81.67	89.98	90.23	88.60	86.89	88.19
MnO	2.11	2.21	2.12	2.04	2.02	2.22	2.07	2.03	0.94	0.35	0.42	0.58	0.68	0.62
MgO	0.03	0.01	0.02	0.02	0.02	–	–	0.04	0.005	0.028	0.047	0.019	–	0.027

Table 7
Chemical composition (wt%) of accessory phases (ilmenite - magnetite solid solution series).

Magnetite-Ilmenite solid solution														
Spots	1	2	3	4	5	6	7	8	9	10	11	12	13	14
SiO_2	0.10	0.08	0.20	0.01	0.06	5.78	0.73	3.76	0.02	–	–	0.10	0.07	4.55
TiO_2	4.76	4.71	5.25	50.75	3.82	7.71	6.68	21.30	50.52	50.28	7.24	5.98	5.33	14.72
Al_2O_3	0.13	0.62	0.07	0.03	–	0.74	0.10	0.49	–	0.01	0.54	0.73	–	0.83
Cr_2O_3	–	0.01	–	–	0.01	0.06	0.03	0.03	–	–	0.01	–	0.01	0.01
FeO	89.22	87.72	89.07	46.36	90.43	76.39	86.18	66.99	45.76	45.4	86.7	84.81	88.28	71.62
MnO	0.44	0.48	0.46	4.01	0.30	0.15	0.53	1.40	3.96	3.62	0.67	0.55	0.44	0.79
MgO	0.05	–	–	–	–	–	–	0.26	0.03	0.01	0.01	0.02	–	0.12
CaO	–	–	0.07	0.01	–	5.00	0.74	2.58	–	–	–	–	0.06	3.39

characterized by $(Ca, Na)^B > 1$, $(Na)^B < 0.5$ and $\left(\frac{Mg}{Mg+Fe^{2+}}\right) < 0.5$ indicating their calcic-ferroan affinity (Yavuz, 2007). The amphiboles in the pink granite varieties of Dharwad granitoids shows significant enrichment of Ti ($\geq$ 3.1 apfu) compared to grey granites ($\leq$ 0.16 apfu) and quartz-monzodiorite ($\leq$ 0.13 apfu) (Table 5). Based on the amphibole classification scheme of Leake et al. (1997), the studied amphiboles are compositionally classified as ferroedenite and sadanagaite.

5.1.4. Pyroxene

Pyroxene is an essential minor mineral phase in the studied quartz-monzodiorites. However, occasional occurrence of clinopyroxene are seen in granites in the study area. One such clinopyroxene (Fig. 8e) from the pink granite was analyzed to determine its crystal chemistry. The crystal is anhedral with rounded to sub-rounded grain boundary and exhibits inter-growth texture with lath-shaped plagioclase crystal (Fig. 8). The pyroxene is represented by augite ($Wo_{42}En_{33}Fs_{25}$, Lindsley, 1983). The crystal has uniform composition (Table 5).

5.1.5. Titanomagnetite-ilmenite

Ilmenite crystallizes as discrete grains contemporaneously with titaniferous magnetite in most magmas. However, exsolution of titaniferous magnetite to discrete grains of ilmenite and magnetite may occur due to unmixing of the titaniferous magnetite (Vincent and Phillips, 1954; Buddington and Lindsley, 1964). Exsolution of titaniferous magnetite to discrete grains of ilmenite and magnetite resulting from the oxidation of pure ulvospinel or magnetite-ulvospinel solid-solutions will have TiO_2 content less than that of pure Fe_2TiO_4 (i.e. 36 wt%). Therefore, primary ilmenite crystallized as discrete grains will have TiO_2 values $\geq$36 wt% (Buddington and Lindsley, 1964).

Discrete crystals of titanomagnetite and ilmenite with subordinate magnetite-ilmenite solid solution series are the dominating accessory mineral phases present in all the varieties of the studied granitoids. Discrete crystals of ilmenite with high Ti content (>49 wt%) than Fe^{2+} are noticed in quartz-monzodiorite (Table 6). Similarly, discrete crystals of magnetite with thin bands of ilmenite are also present in quartz-monzodiorite (Table 6). However, majority of the opaque oxides in the grey and pink granites are the magnetite-ilmenite solid solution series (Table 7) with inclusions of amphibole.

5.2. Pressure-temperature conditions

The calculated minimum and maximum pressure (P) and temperature (T) values of the Dharwar granitoids are given in Table 8.

5.2.1. Pressure

Al-in-amphibole geobarometer was used to estimate the pressure of emplacement of the Dharwad granitoids. Pressure was calculated using revised temperature corrected expression given by Anderson and Smith (1995): $P(\pm 0.6kbar) = \left(4.76Al - 3.01 - \frac{T-675}{85}\right) \times (0.530Al + 0.005294(T-675))$, which incorporates the effects of temperature and oxygen fugacity. Estimated pressure values for the studied quartz-monzodiorite range between 3.09–4.36 kbar (av. 3.73 kbar) while for granites it is between 0.89 and 1.88 kbar (av. 1.39 kbar). Assuming an average crustal specific gravity of 3.0 g/cm^3, an approximate emplacement depth varying between 10–15 km (av. 12.5 km) for quartz-monzodiorite and 3–6 km (4.5 km) for granite has been calculated. Interestingly, estimated pressure values for one of the amphibole crystal from the studied pink granites range between 3.46–4.78 kbar (av. 4.12 kbar) and a calculated emplacement depth varies between ~12 to 16 km (14 km). This pressure and depth estimates are similar to that of quartz-monzodiorite rather than the grey or pink granites.

Clinopyroxene barometry (Putirka, 2008) was used to estimate the pressure conditions at which the pyroxene crystal in the studied pink granite was crystallized. Results of the clinopyroxene barometer indicate that the pyroxene in pink-granite crystallized between 4.22 and 6.32 kbar (av. 5.27 kbar) and at a depth of approximately 14–21 km (av. 17.5 km).

Table 8
Calculated pressure and temperature (P-T) values of the Dharwar Granitoids.

Sl. No.	Rock/Mineral	Pressure (kbar)		Temperature (°C)	
		(Min.)	(Max.)	(Min.)	(Max.)
1	Quartz-monzodiorites	3.09	4.36	638 ± 40	972 ± 40
2	Granites	0.89	1.88	640 ± 40	720 ± 40
3	Amphibole in pink granite	3.46	4.78	1095 ± 40	
4	Pyroxene in pink granite	4.22	6.32	1135 ± 40	

5.2.2. Temperature

Temperatures were calculated using the amphibole-plagioclase (Holland and Blundy, 1994), Ti-in-amphibole (Otten, 1984), single pyroxene (Putirka, 2008) and two-feldspar (Whitney and Stormer, 1977) geothermometers.

The re-calibrated formulation based on edenite-richterite reaction was used to calculate temperature in amphibole-plagioclase thermometer (Holland and Blundy, 1994). The crystallization temperatures of 972 ± 40 °C to 638 ± 40 °C from core to rim (with an average temperature of 805 ± 40 °C) respectively have been obtained for an amphibole crystal from the quartz-monzodiorite. An amphibole crystal from the grey granite have yielded a narrow range of crystallization temperatures of 720 ± 40 °C to 640 ± 40 °C from core to rim (with an average temperature of 680 ± 40 °C) respectively. Further, an amphibole crystal from the grey granite have yielded a homogeneous crystallization temperature of 1095 ± 40 °C.

Ti-in-amphibole is an accurate measure of temperature as long as Ti-bearing phases (ilmenite and/or titanite) are present in the rocks (Helz, 1973; Otten, 1984; Ernst and Liu, 1998). Temperature was calculated using the calibration given by Otten (1984): $[T\ (^{\circ}C) = (1204 \times Ti) + 545]$, where Ti is the number of Ti cations per unit formula (23 oxygens), which is applicable for T < 970 °C. An average crystallization temperature of 984 °C have been obtained for an amphibole crystal from the quartz-monzodiorite. An amphibole from the grey granite have yielded a narrow range of crystallization temperatures of 738 °C to 617 °C from rim to core (with an average temperature of 686 °C). This temperature range is almost similar to that obtained using amphibole-plagioclase thermometer for the grey granite.

A single-pyroxene thermometer (Putirka, 2008) yielded crystallization temperature of 1135 ± 40 °C for the clinopyroxene (augite) crystal in the studied pink granite.

Two-feldspar thermometer (Whitney and Stormer, 1977) has yielded crystallization temperatures of 1047 ± 40 °C to 604 ± 40 °C (av. 857 ± 40 °C) for the first generation plagioclase feldspar and 687 ± 40 °C to 491 ± 40 °C (av. 556 ± 40 °C) for the second generation plagioclase feldspar.

5.2.3. Oxygen fugacity (f_{O2})

Presence of euhedral titanite and magnetite as early crystallizing phases in felsic rocks indicates that the magma was relatively oxidized (Enami et al., 1993). The assemblage titanite + magnetite + quartz in granitoid rocks permits an estimate of relative oxygen fugacity (Wones, 1989). f_{O2} can be estimated using the calibration given by Wones (1989), $logf_{o_2} = -\frac{30930}{T} + 14.98 + 0.142 \times \frac{(P-1)}{T}$ where T is the temperature (in Kelvins) and P is pressure (in bars). Temperatures and pressures estimated from two-feldspar thermometer and aluminum-in-hornblende barometer respectively were used in these calculations. The studied quartz-monzodiorite yields intermediate f_{O2}values ranging between -7.98 and -8.12 suggesting reducing conditions, while granite yields high f_{O2}values ranging between -17.23 and -17.54 indicating oxidizing conditions. It is interesting to note that one of the amphibole (sadanagite) crystal in the grey granite has yielded the lowest f_{O2}values ranging between -7.01 and -7.30 indicating its reducing environment of crystallization, similar to that in quartz-monzodiorite. Therefore, T-f_{O2} estimates for the Dharwad granitoids indicate a variable redox conditions during magma crystallization.

5.2.4. Significance of magmatic epidote

Epidotes in magmatic rocks have two origins - primary and secondary. The epidote crystallized during the cooling of magma is called primary magmatic-epidote while alteration of plagioclase, biotite and amphibole results in secondary epidote (Dawes and Evans, 1991; Vyhnal et al., 1991; Perkins, 1998). Euhedral epidote overprinting biotite, epidote overgrowths on euhedral allanite, resorption of hornblende with subsequent precipitation of epidote, wormy inter-growths with plagioclase, involvement of epidote in magmatic flow banding and occurrence of epidote in rocks that otherwise lack secondary alteration are some of the petrographic criteria by which magmatic epidote can be distinguished from the epidote that forms by subsolidus (deuteric) reaction and hydrothermal or metamorphic crystallization (Vyhnal et al., 1991; Dawes and Evans, 1991). Chemically, epidotes formed from the breakdown of plagioclase are Fe-poor, while epidotes replacing biotite and amphibole (along with chlorite) are distinctly Fe-rich than the magmatic epidotes (Speer, 1980; Dawes and Evans, 1991). Further, magmatic epidotes range from Ps_{25} to Ps 33 $\left[pistacite(Ps) = \frac{Fe^{3+}}{Fe^{3+}+Al}\right]$, while epidotes formed from alteration of plagioclase ranged from Ps_0 to $Ps_{24}$and those formed by alteration of biotite ranged between Ps_{36} and Ps_{48} (Tulloch, 1979, 1986; Vyhnal et al., 1991).

Magmatic epidotes are known to be in equilibrium with granitic melts at pressures above 6–8 kbar (Naney, 1983; Zen and Hammarstrom, 1984, 1988; Dawes and Evans, 1991). However, Vyhnal et al. (1991) have reported magmatic zircons in calc-alkaline plutons emplaced at pressures of 2.8 ± 0.5 kbar or greater. The probable reasons for the occurrence of epidotes in magmas crystallized at shallow crustal levels are either the epidote crystallizes at a large pressure interval (between 2 and 8 kbar) or the rate of dissolution of epidote in granitic magmas at pressures <6 kbar is slower than the magma ascent rate. There are no proven experiments to support the former assumption. However, Brandon et al. (1996), based on their experiments on the rate of epidote dissolution in granitic magmas, demonstrated that the presence of magmatic epidotes in low pressure granitic rocks could be due to the rapid upward transportation of epidote crystal bearing granitic magmas from the deep crust. The rapid movement of the high-pressure crystal-laden magma in the form of dykes (rather than diapirs) prevents complete resorption of epidote crystals (see Brandon et al., 1996).

The euhedral epidotes in the low pressure Dharwad granitoids exhibit inter-growth texture with plagioclase crystals (Fig. 6). They are present as accessory phases in all three varieties of Dharwad granitoids. Occasional intergrowth of subhedral to euhedral grains of epidote on biotite and inter-crystalline growth between plagioclase are not uncommon. Microprobe analysis shows homogeneous composition of the epidote crystal (inter-grown with plagioclase) from core to rim with no enrichment of Fe (Ps_{29} to Ps_{30}) (Table 9). The textural and chemical characteristics of the studied epidote points to its magmatic origin, at mid-deep crustal levels. The rapid upward movement of the epidote bearing melt is also evident.

5.3. CSD

The quartz monzodiorite rocks show a hump shaped pattern (Fig. 10) which indicates increment in population of smaller grains up to a size of 0.5 mm–1 mm in their longest axis followed by continuous reduction in population as the crystals get bigger. The negative slope of the curve does not fit with the linear regression line and shows a concave up type pattern. The grey granites show a negative slope which overlaps on the linear regression line (Fig. 10) suggesting a gradual increase in crystal size with respect to the crystal population. The pink granites show a similar pattern as that of the quartz monzodiorite (Fig. 10). The plagioclase crystal populations increase with crystal size up to 1 mm size followed by gradual reduction of crystal size with respect to population similar to the grey granite. Marsh (1988) suggested that presence of a straight line in the crystal size distribution curve implies constant condition. Fractionation processes cause CSD plot to be curved but their intercepts are nearly same (Kamaci and Altunkaynak, 2019). Similarly, Higgins (1996) interpreted the concave up shape of CSD curve to be the result of magma mixing (Deb and Bhattacharyya, 2018; Kamaci and Altunkaynak, 2019). However, a curved CSD plot can also form due to an abrupt change in cooling environment. Higgins (2011) demonstrated that textural coarsening of minerals can result in kinked or hump shaped

Table 9
Chemical composition (wt%) of epidote.

Spots	1	2	3	4	5	6	7	8	9	10
SiO_2	37.12	36.98	37.06	37.17	36.75	37.04	37.36	36.95	37.19	37.07
Al_2O_3	22.22	22.12	22.05	22.53	22.11	22.31	22.05	21.85	22.17	22.56
FeO	13.21	13.2	13	12.87	13.13	13.45	13.36	13.17	13.27	13.09
MgO	0.03	0.03	0.01	0.04	0.01	–	–	–	0.02	0.01
MnO	0.11	0.12	0.15	0.36	0.19	0.15	0.08	0.14	0.14	0.06
CaO	22.78	22.69	22.79	22.36	22.28	22.91	22.96	22.73	22.74	22.82

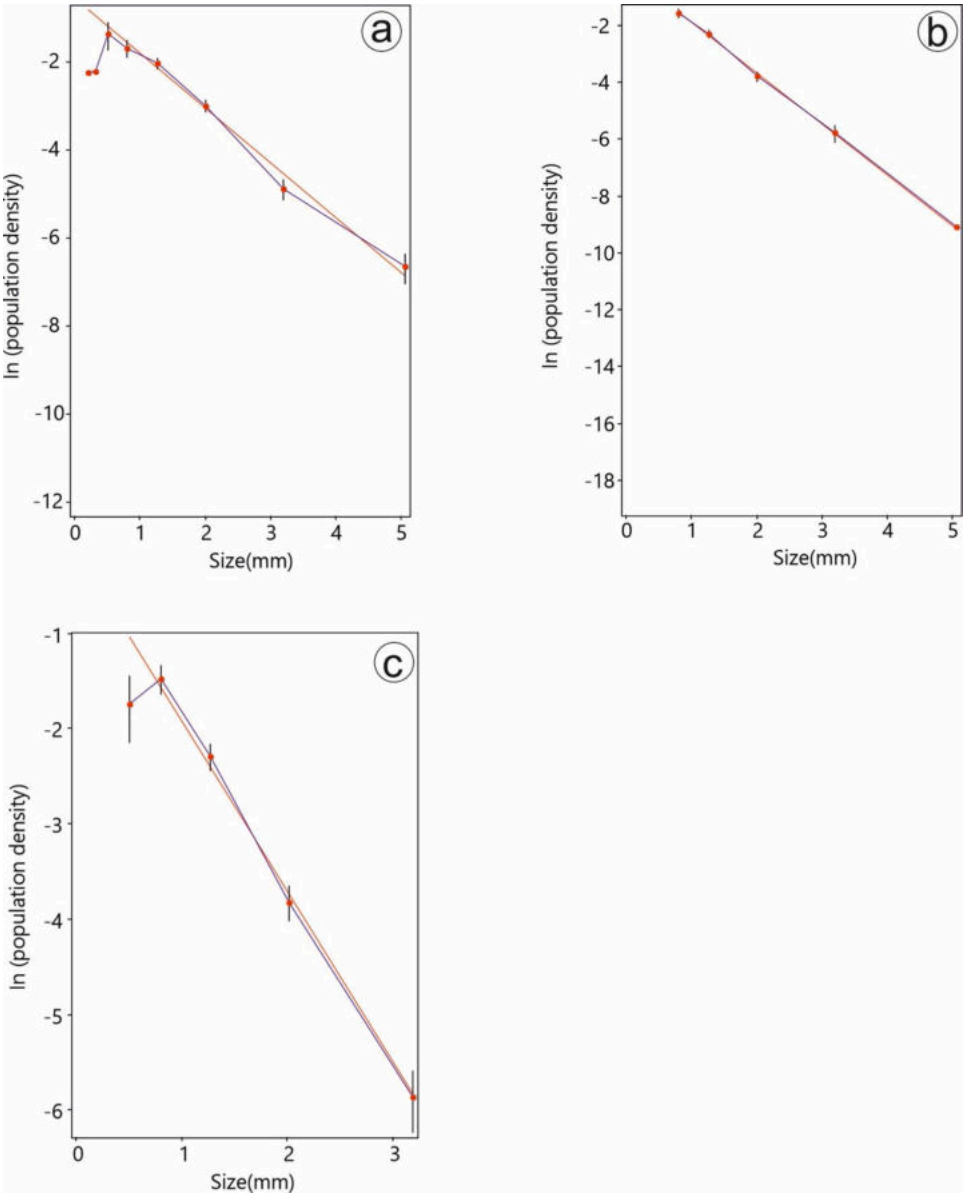

Fig. 10. Crystal size distribution curves of (a) quartz-monzodiorite; (b) grey- granite; and (c) pink granite.

CSD curves which represents that the larger crystals have grown at the expense of smaller ones. The CSD plots of the quartz monzodiorite display both hump shaped curves (at smaller crystals) and concave up shaped curve (towards larger crystals) which we interpret to be the result of magma mixing and textural coarsening (Higgins, 1996; Deb and Bhattacharyya, 2018; Kamaci and Altunkaynak, 2019). The grey granitoids display a straight line without any change in the shape of the curve which indicates an equilibrium crystallization condition for the generation of the grey granitoids (Marsh, 1988). The pink granites show a kink shaped curvature in the smaller sized crystals similar to the quartz monzodiorite and display straight line in the coarser grains. The CSD curve of the pink granites indicates textural coarsening during equilibrium crystallization conditions.

5.4. Bulk-rock chemistry

The Dharwad granitoids are intermediate to felsic in composition with a narrow range of SiO_2(55.4–65.6 wt%; Tables 10 and 11), low to

Table 10
Major-oxide analysis of quartz-monzodiorite and grey-granite.

Sample	Q1	Q2	DG-12	G1	G2	DG-1	DG-2	DG-3	DG-4	DG-5	DG-6	DG-7	DG-8	DG-9	DG-10	DG-11	DG-13	DG-14	DG-15
	Quartz-monzodiorite			Grey-granite															
SiO_2	55.38	55.51	54.48	65.56	64.72	66.2	66.99	67.28	66.48	65.74	66.6	66.88	67.36	66.42	66.54	66.29	65.45	65.1	66.44
TiO_2	1.57	1.45	1.44	0.77	0.82	0.78	0.77	0.67	0.69	0.82	0.72	0.66	0.67	0.74	0.68	0.77	0.89	0.912	0.72
Al_2O_3	16.16	16.18	16.03	15.15	15.34	15.32	15.3	15.42	15.23	15.36	15.26	15.46	15.42	15.27	15.26	15.55	15.42	15.34	15.43
MnO	0.12	0.11	0.12	0.09	0.09	0.08	0.08	0.07	0.08	0.09	0.09	0.07	0.07	0.08	0.08	0.08	0.09	0.09	0.08
Fe_2O_3	9.43	9.35	10.55	5.6	6	4.67	4.7	4.44	4.77	5.45	4.81	4.55	4.51	5.04	4.56	4.98	5.56	5.86	4.95
CaO	7.34	7.69	6.78	2.32	2.75	2.34	2.21	2.14	2.2	2.65	2.36	2.29	2.25	2.39	2.16	2.36	2.74	2.82	2.38
MgO	3.91	3.86	4.85	0.76	0.86	0.66	0.66	0.66	0.61	0.76	0.69	0.64	0.65	0.67	0.58	0.68	0.8	0.89	0.71
Na_2O	4.03	3.92	3.74	4.93	4.89	4.87	4.87	4.95	4.85	4.84	4.89	4.92	4.89	4.83	4.75	4.91	4.87	4.84	4.98
K_2O	1.46	1.38	1.59	3.81	3.66	3.95	4.01	3.96	3.99	3.85	3.98	4.05	4.13	3.98	4.05	3.94	3.72	3.66	3.91
P_2O_5	0.21	0.21	0.2	0.22	0.27	0.23	0.24	0.23	0.21	0.29	0.23	0.2	0.22	0.24	0.22	0.27	0.31	0.34	0.25
Na_2O/K_2O	2.76	2.84	2.35	1.29	1.34	1.23	1.21	1.25	1.21	1.26	1.23	1.21	1.18	1.21	1.17	1.25	1.31	1.32	1.27
Na + K/Al	0.49	0.47	0.48	0.85	0.82	0.85	0.86	0.85	0.86	0.83	0.86	0.86	0.86	0.85	0.85	0.84	0.82	0.82	0.85
ASI	0.59	0.57	0.62	0.8	0.78	0.8	0.82	0.83	0.81	0.78	0.8	0.81	0.81	0.8	0.82	0.81	0.79	0.78	0.8
K_2O/Na_2O	0.36	0.35	0.43	0.77	0.75	0.81	0.82	0.8	0.82	0.8	0.81	0.82	0.84	0.82	0.85	0.8	0.76	0.76	0.79
Fe_2O_3+MgO + MnO + TiO_2	15.03	14.77	16.96	7.22	7.77	6.19	6.21	5.84	6.15	7.12	6.3	5.92	5.91	6.53	5.89	6.52	7.34	7.76	6.45
Fe*	0.71	0.71	0.69	0.88	0.87	0.88	0.88	0.87	0.89	0.88	0.88	0.88	0.87	0.88	0.89	0.88	0.87	0.87	0.88

moderate K_2O (1.38–4.07 wt%) and considerably higher Na_2O (3.924.93 wt%). They have moderate to higher alumina content [Al_2O_3> 15 wt%] and higher alkali ratio [$Na_2O/K_2O > 1$], characteristic of transitional tonalite-trondhjemite-granodiorites (TTGs) (Champion and Smithies, 2003). These granitoids have moderate alkali contents (5.30–8.84 wt%) and are spread across the fields of diorite and granite in the total-alkali silica (TAS; Cox et al., 1979) diagram (Fig. 11). The quartz-monzodioritic variety of Dharwad granitoids occupy diorite field while the granitic varieties fall on the boundary line between granodiorite and granite (Fig. 11). The granitoids plot in the medium to high-K fields of the calc-alkaline series in the K_2O vs. SiO_2 diagram (Fig. 11b; Peccerillo and Taylor (1976)). The MgO content of the quartz-monzodiorites is higher (3.86–3.91 wt%) than the granites (0.74–0.86 wt%) due to the predominance of mafic silicate phases in the former. TiO_2, Al_2O_3, Fe_2O_3, MgO and CaO shows decreasing while Na_2O and K_2O shows increasing trend from quartz-monzodiorites to granites in the Harker variation diagrams (Supplementary Fig. 1). The Dharwad granitoids have Fe* (Fe-number; Frost et al., 2001) greater than 0.5 (and < 1) and have higher mole proportions of Fe than Mg and are hence, classified as ferroan (Frost et al., 2001). These rocks are metaluminous with molar $\frac{Na+K}{Al} < 1$ and ASI (Alumina Saturation Index) < 1 (Fig. 11c; Frost et al., 2001; Frost and Frost, 2008). All these features indicate that the Dharwad granitoids do not represent mantle-derived primary magma composition.

The transitional elements (Co, Ni and V) are enriched in quartz-monzodiorite due to the dominant mafic silicate phases in them. In the primitive mantle normalized multi-element diagram, except Sr, the analyzed compatible elements (Rb and Cs) and the incompatible elements (Nb, Ta, Zr, Hf and Y) shows enrichment in granites than quartz-monzodiorites (Fig. 12a (Sun and McDonough, 1989); Tables 12 and 13). There is no particular increasing or decreasing trends exhibited by the trace elements between the grey and pink granites, however, in general, the incompatible elements tend to increase in pink granites (Supplementary Fig. 2; Table 13). The total rare earth element concentration increases from quartz-monzodiorite ($\sum$REE =112 ppm) to granite ($\sum$REE = av. 231 ppm). The quartz-monzodiorite display light REE (LREE) fractionation $\left[\left(\frac{La}{Sm}\right)_N = 2.48\right]$ with no europium anomalies $\left[\left(\frac{Eu}{Eu}\right)^* = 1\right]$ and negligible heavy REE (HREE) depletion $\left[\left(\frac{Gd}{Yb}\right)_N = 2.06\right]$ (Fig. 12b; Boynton, 1984). The fractionation trends of the granites are similar to the quartz-monzodiorite, except the moderate negative europium anomalies $\left[\left(\frac{Eu}{Eu}\right)^* = 0.85 - 0.69\right]$ in the former (Fig. 12b).

6. Discussions

6.1. Petrogenesis

Due to the predominant crustal reworking process, the late Archean period has witnessed extensive felsic magmatism globally, and the Dharwar Craton is no exception to it (Sylvester, 1994; Jayananda et al., 2006). These late Archean granitoids cover a wide range of petrographic and mineralogical compositions and are most commonly grouped under following four categories (see Laurent et al., 2014): (i) volumetrically-dominant and juvenile tonalite-trondhjemite-granodiorites (TTGs), whose geochemistry is consistent with an origin through partial melting of meta-igneous mafic rocks at various pressures; (ii) Mg-, Fe- and K-rich, metaluminous (monzo) diorites and granodiorites, referred to as sanukitoids senso lato (s.l.), which are derived primarily from hybridization between mantle peridotite and a component rich in incompatible elements; (iii) peraluminous and K-rich biotite- and two-mica granites, formed through melting of older crustal lithologies; and (iv) hybrid high-K granites with mixed characteristics from the above three groups. Few noted examples of granitoids of Dharwar

Table 11
Major-oxide analysis of pink-granite.

Sample	P1	P2	DG-16	DG-17	DG-18	DG-19	DG-20	DG21	DG22
SiO_2	64.69	64.73	65.25	65.51	65.63	66	66.4	65.92	66.79
TiO_2	0.81	0.83	0.76	0.78	0.75	0.76	0.71	0.71	0.68
Al_2O_3	15.65	15.96	15.76	15.83	15.98	16.25	15.64	16.04	15.85
MnO	0.1	0.09	0.09	0.09	0.09	0.09	0.09	0.09	0.08
Fe_2O_3	5.61	5.6	4.8	4.93	4.81	4.85	4.56	4.74	4.38
CaO	2.83	2.56	2.79	2.93	2.78	2.53	3.05	2.81	2.49
MgO	0.84	0.74	0.641	0.66	0.63	0.6	0.7	0.7	0.61
Na_2O	4.72	4.77	4.7	4.65	4.69	4.51	4.64	4.42	4.6
K_2O	3.8	4.07	4.13	4.22	4.26	4.14	3.84	4.21	4.17
P_2O_5	0.2	0.22	0.22	0.24	0.22	0.22	0.22	0.23	0.2
Na_2O/K_2O	1.24	1.17	1.14	1.1	1.1	1.09	1.21	1.05	1.1
Na + K/Al	0.8	0.82	0.83	0.83	0.83	0.79	0.8	0.8	0.82
ASI	0.78	0.81	0.78	0.76	0.78	0.84	0.76	0.8	0.82
K_2O/Na_2O	0.81	0.85	0.88	0.91	0.91	0.92	0.83	0.95	0.91
Fe_2O_3+MgO + MnO + TiO_2	7.36	7.26	6.29	6.46	6.28	6.3	6.06	6.23	5.75
Fe*	0.87	0.88	0.88	0.88	0.88	0.89	0.87	0.87	0.88

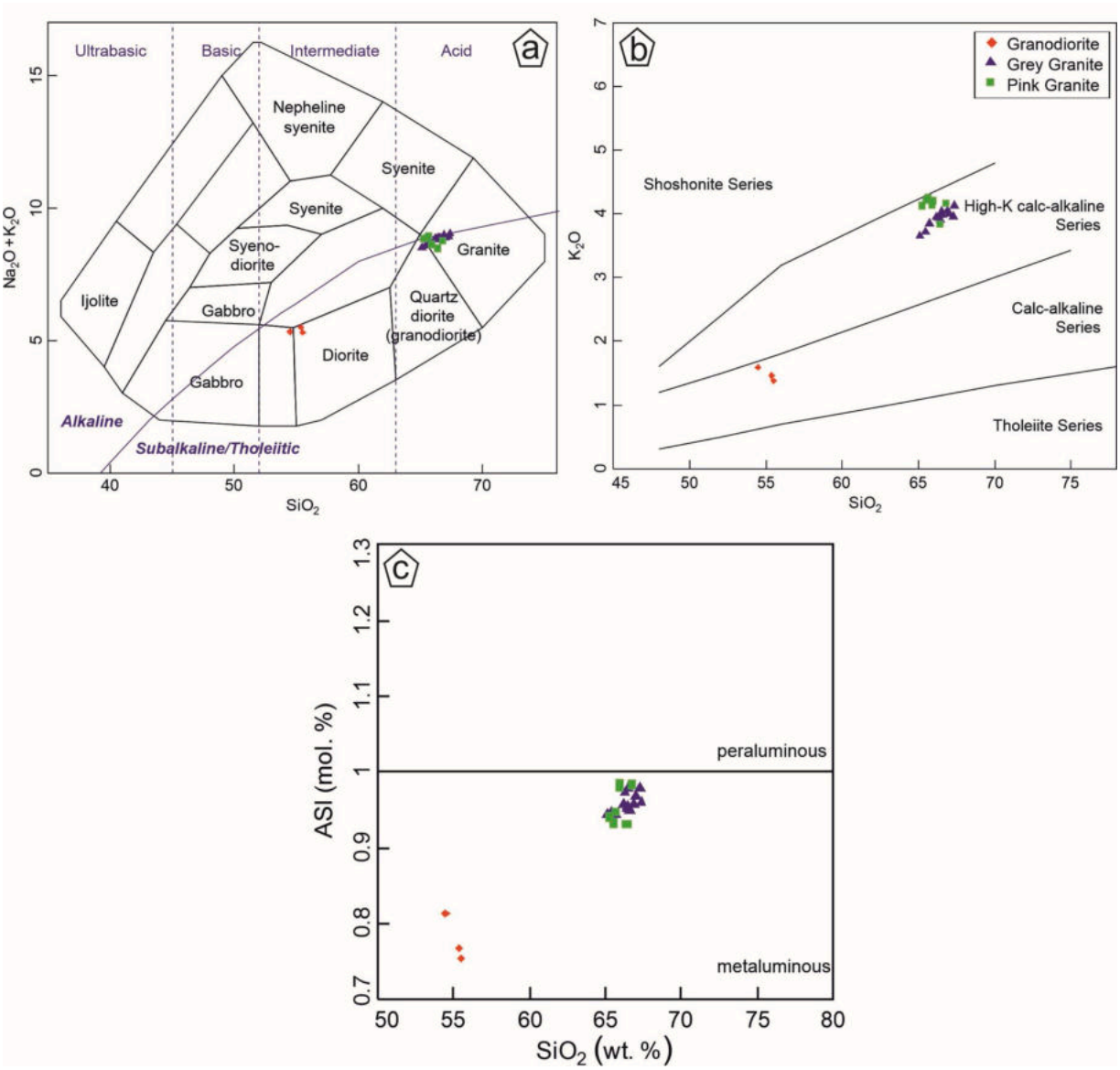

Fig. 11. (a) Total-alkali silica diagram of Cox et al. (1979); (b) SiO_2-K_2O plot of Peccerillo and Taylor (1976); (c) SiO_2-ASI (Alumina-Saturation Index) plot of Frost and Frost (2008).

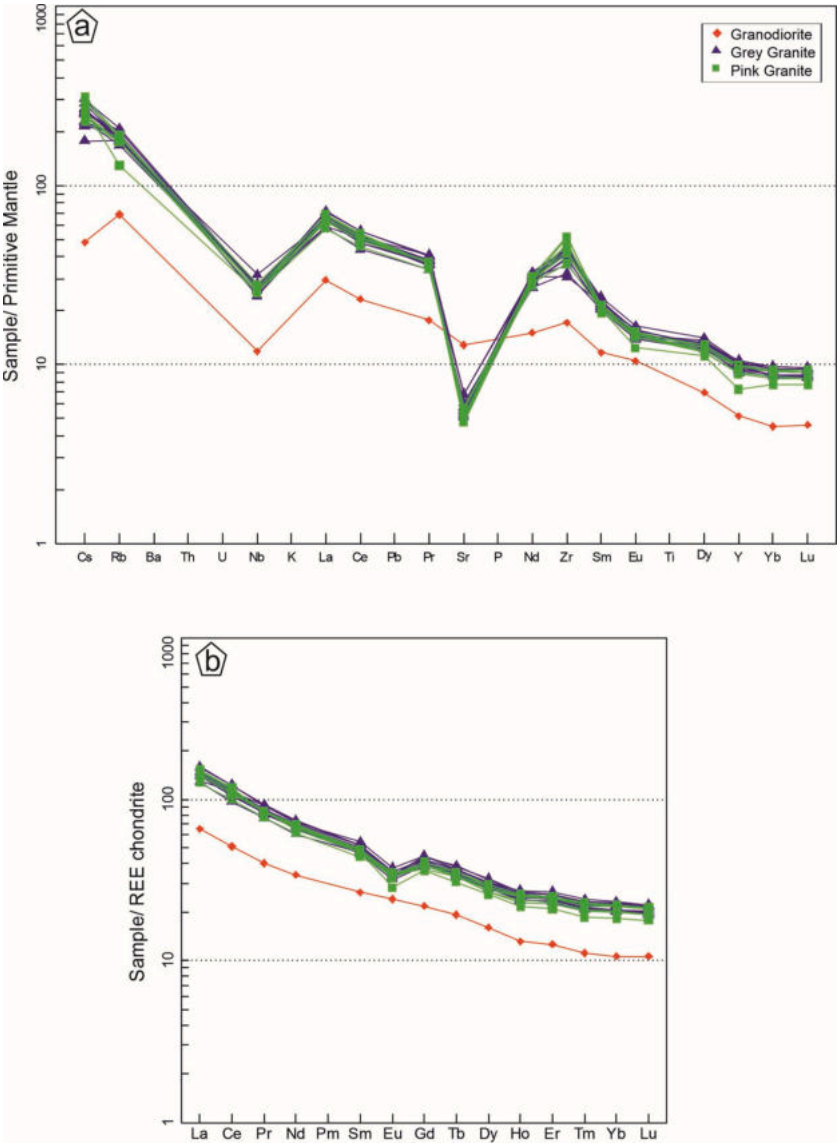

Fig. 12. (a) Chondrite normalized REE patterns (Boynton, 1984); (b) Primitive mantle-normalized multi-element patterns (Sun and McDonough, 1989).

Craton that fall into these four groups are: (i) TTG type - Peninsular Gneisses, Krishnagiri tonalites and the gneisses in the HuttiGurgunta area; (ii) sanukitods s.l type - Dod gneisses, Bisanattam granitoid, mafic phases of Closepet batholith; (iii) biotite- and two-mica granite type - Bangalore leucogranite, Kadri-Lepakshi-Madanapalle-Nandi Hills granites, Kolar granodiorite and Guramkonda-Vendodu granites; and (iv) hybrid granitoid type - felsic phases of Closepet batholith, Arasikere-Banavara granites, Chitradurga-Jampalnaikankote-Hosdurga granites and transitional-TTG type granites in Hutti-Gurgunta area (Jayananda et al., 1995, 2006; Moyen et al., 2001, 2003; Prabhakar et al., 2009).

6.1.1. *Relative age of the Dharwad Granitoids*

The granitoids reported in this study are the first ever reported younger granitoid plutons from the northern part of the Shimoga greenstone belt in the Dharwar Foreland region. As noted earlier, these granitoids lack structural deformation that are conspicuous in the litho units of the greenstone belt and cut sharply across the planar fabric of the youngest units of the Shimoga greenstone belt (Fig. 2), i.e. thick sequences of metasediments (metagreywackes and banded iron formations). Also, these granitoids along with the host metasediments are overlain by the Proterozoic Kaladgi sedimentary rocks (Harinadha Babu et al., 1981; Chadwick et al., 2000; Ugarkar et al., 2012; Chadwick et al., 1991). The host metasediments belongs to the Ranibennur Formation of the Lower Chitradurga Group of Dharwar Supergroup stratigraphy (Table 14). The relative age of the metasediments of Ranibennur Formation is ~2600 Ma (Ramakrishnan and Vaidyanadhan, 2010; Chadwick et al., 2000), while the youngest dated rocks in Shimoga greenstone belt are 2.61 Ga old felsic volcanics that belongs to Lower Chitradurga Group (Nutman et al., 1996). Based on the field relation between the studied granitoids and the associated litho units, the studied granitoids are presumed to be approximately 2580–2560 Ma old.

6.1.2. *Petrographic evidences*

The Dharwad granitoids consist of composite magmatic complex that is made up of dominant phase of leucocratic granites, subordinate mesocratic quartz-monzodiorite and occasional mafic magmatic enclaves of dioritic-granodioritic composition. The complex is undeformed, devoid of large K-feldspar phenocrysts and are not associated with ultrapotassic mafic intrusions. These observations suggests that the studied granitoids are not derived from a single crustal lithology rather they have hybrid genetic history (Laurent et al., 2014). Amphiboles (ferroedenite and sadanagaite) are the dominating mafic phase with subordinate clinopyroxene (augite) while plagioclase (~60%) dominates the felsic phase followed by quartz (~20%) and K-feldspar

Table 12
Trace-element analysis of Dharwad Granitoids (GD-Quartz monzodiorite; GG-Grey granite).

Sample	DG12	DG1	DG2	DG3	DG5	DG6	DG7	DG8	DG9	DG10	DG11	DG13	DG14	DG15
	GD	GG												
Co	31	5	5	5	6	5	5	5	5	5	6	7	7	5
Ni	109	0.32	0.19	0.03	0.27	0.37	4.13	0.23	0.05	0.27	0.05	0.46	0.64	0.19
V	306	25	26	23	29	23	22	23	24	22	26	33	36	24
Rb	44	106	129	129	113	122	123	123	118	132	116	113	111	113
Sr	271	111	115	118	121	112	109	115	107	109	129	144	143	123
Cs	0.38	1.81	1.99	2.02	1.4	1.7	1.73	1.77	2.12	2.4	2.04	2.26	2.11	2.41
Ta	0.42	0.98	0.95	0.92	0.91	0.95	0.86	0.87	1.01	1.02	0.98	1.05	0.97	0.95
Nb	8	20	19	19	19	18	17	17	19	19	19	23	20	19
Zr	191	478	459	499	474	404	441	496	490	484	362	346	494	436
Hf	3.42	8.6	8.67	8.8	8.66	7.77	8.25	9.11	9.35	9.5	7.35	6.62	9.48	8.13
Y	23	44	46	46	46	44	42	44	46	48	41	44	47	43
La	20.31	40.46	48.52	49.33	45.17	45.42	43.67	43.77	46.41	46.33	39.57	44	46.42	43.42
Ce	41.17	90.24	99	98.94	91.89	92.58	88.49	91.49	84.28	88.87	78.04	89.47	90.8	84.22
Pr	4.88	9.85	11.07	11.23	10.55	10.62	10.06	9.94	10.38	10.51	9.32	10.09	11.16	10.05
Nd	20.37	39.93	44.08	44.14	42.51	40.99	39.43	39.91	39.38	41.42	36.47	41.51	43.09	39.32
Sm	5.15	9.47	10.01	10.15	10.05	9.42	8.94	9.36	9.67	9.68	9.05	9.74	10.55	9.24
Eu	1.76	2.38	2.45	2.46	2.6	2.38	2.33	2.43	2.39	2.46	2.54	2.62	2.75	2.5
Gd	5.64	10.35	11.28	11.4	10.93	10.87	10.02	10.17	10.89	10.49	10.03	10.84	11.55	10.5
Tb	0.91	1.63	1.83	1.75	1.73	1.58	1.59	1.56	1.74	1.7	1.61	1.64	1.8	1.67
Dy	5.13	9.36	10.09	9.68	9.66	9.17	8.94	9.02	9.75	9.79	9.23	9.26	10.31	9.43
Ho	0.94	1.84	1.9	1.87	1.83	1.81	1.69	1.78	1.86	1.94	1.71	1.79	1.9	1.76
Er	2.64	5.19	5.4	5.39	5.25	5.11	4.93	5.16	5.41	5.57	4.81	5.02	5.39	5.09
Tm	0.36	0.72	0.74	0.72	0.72	0.69	0.68	0.71	0.75	0.77	0.67	0.68	0.74	0.69
Yb	2.22	4.53	4.62	4.64	4.5	4.3	4.2	4.55	4.77	4.82	4.22	4.21	4.65	4.33
Lu	0.34	0.67	0.7	0.69	0.67	0.64	0.62	0.69	0.71	0.71	0.63	0.63	0.7	0.65
∑REE	111.82	226.62	251.69	252.39	238.06	235.58	225.59	230.54	228.39	235.06	207.9	231.5	241.81	222.87
$(La/Sm)_N$	2.48	2.69	3.05	3.06	2.83	3.03	3.07	2.94	3.02	3.01	2.75	2.84	2.77	2.96
$(Gd/Yb)_N$	2.06	1.85	1.97	1.99	1.96	2.05	0.93	1.81	1.85	1.76	1.92	2.08	2.01	1.96
$(La/Yb)_N$	6.17	6.02	7.08	7.17	6.77	7.12	7.01	6.49	6.56	6.48	6.32	7.05	6.73	6.76
(Eu/Eu)*	1	0.74	0.7	0.7	0.76	0.72	0.75	0.76	0.71	0.75	0.82	0.78	0.76	0.78

Table 13
Trace-element analysis of Dharwad Granitoids.

Sample	DG16	DG17	DG18	DG19	DG20	DG21	DG22
Pink granites							
Co	5	5	5	5	5	5	4
Ni	0.39	0.05	0.17	0.18	0.17	0.34	0.58
V	23	25	23	23	23	24	21
Rb	111	111	112	112	82	121	118
Sr	119	118	121	100	102	104	109
Cs	1.89	1.79	1.93	1.99	2.14	2.47	2.35
Ta	0.87	0.89	0.88	0.89	0.93	0.94	1.03
Nb	18	19	18	18	18	20	19
Zr	542	572	483	466	409	579	522
Hf	9.65	10.51	9.02	8.82	7.32	10.04	9.34
Y	44	44	40	41	33	44	45
La	39.35	43.48	44.91	45.07	43.32	46.17	47.52
Ce	80.73	87.47	89.61	90.5	87.08	94.02	95.29
Pr	9.38	10.25	10.19	10.32	10.34	10.14	10.08
Nd	37.05	40.37	40.23	40.54	38.69	42.15	41.9
Sm	8.58	9.48	9.1	9.49	9.05	9.16	9.56
Eu	2.51	2.57	2.49	2.39	2.08	2.38	2.5
Gd	9.51	10.06	10.11	10.1	9.35	10.26	10.57
Tb	1.58	1.68	1.56	1.58	1.45	1.6	1.68
Dy	8.81	9.1	8.57	8.62	8.22	9.13	9.47
Ho	1.78	1.79	1.64	1.7	1.54	1.8	1.85
Er	5.14	5.15	4.71	4.9	4.39	5.2	5.19
Tm	0.72	0.7	0.65	0.67	0.6	0.73	0.74
Yb	4.54	4.53	4.13	4.25	3.79	4.55	4.6
Lu	0.67	0.67	0.62	0.62	0.57	0.69	0.69
∑REE	210.35	227.3	228.52	230.75	220.47	237.98	241.64
$(La/Sm)_N$	2.88	2.89	3.1	2.99	3.01	3.17	3.13
$(Gd/Yb)_N$	1.69	1.8	1.98	1.92	2	1.82	1.86
$(La/Yb)_N$	5.84	6.47	7.33	7.15	7.71	6.84	6.96
(Eu/Eu)*	0.85	0.8	0.79	0.75	0.69	0.75	0.76

(~10%) in quartz-monzodiorites. While, the granites consist of almost equal proportions of plagioclase (~33%) and K-feldspar (~31%) with subordinate quartz (~20%). Titanomagnetite, apatite, zircon, ilmenite and magmatic epidote are the accessory phases. Absence of muscovite and limited biotite modal abundance implies that the Dharwad granitoids are not derived from biotite or two-mica granites (Laurent et al., 2014). Further, the presence of magmatic epidote indicates that the source magma of these granitoids were generated at mid-deep crustal

Table 14
Stratigraphic column of Shimoga greenstone belt.

	Harinadha Babu et al. (1981)		Chadwick et al. (1991)	
Late Archean	Chitradurga Group	Ranibennur Formation	Ranibennur Formation Basavapatna Formation	Upper Chitradurga Group
		Medur Formation	Daginkatte Formation Medur Formation	
		Joldhal Formation	Aleshpur Formation	Lower Chitradurga Group
		Jhandimatti Formation	Adrihalli Formation Mushinhal Formation	
	Bababhudan Group Absent		Kalva Rangan Durga Formation Kudrekonda Formation	Bababudan Group
	Peninsular Gneiss-granodiorite and foliated multiphase orthogneisses			
	Sargur Group			

levels.

6.1.3. Textural evidences

Wyllie et al. (1962) regarded acicular apatite as a quench texture which are formed due to rapid cooling of the rock. Hibbard (1991) suggested that presence of mixed apatite morphologies where apatite occur as acicular as well as prismatic crystals are features compatible with magma mixing and mingling. Another important textural feature to be noted in the quartz monzodiorite is mantling of hornblende crystals over quartz which also suggests magma mixing (Hibbard, 1991). Presence of resorbed crystal boundaries of quartz with hornblende and embayment of quartz crystals within hornblende crystals were interpreted to be formed as a result of magmatic corrosion where a previously stable mineral becomes unstable with respect to liquid and begins to dissolve. Mechanism driving such interaction is interpreted to be magma mixing (Vernon, 2018). In light of all these evidences, it is interpreted that the studied quartz monzodiorites of the northern part of the Dharwar foreland region were the product of magma mixing.

The mantling of biotite over amphiboles in the studied grey granites indicate the evolution of relatively more mafic magmas to generate less mafic phases as crystallization proceeded along with a progressive increase in hydrous content (Hibbard, 1991). The inter-growth texture exhibited by quartz and feldspar crystals are formed due to high undercooling conditions originated by reduction of temperature due to rapid accent or addition of volatiles (Vernon, 2018). Few workers interpreted this inter-growth texture to be a product of metasomatism (Vernon, 2018). However, in the absence of any field and laboratory evidences for fluid movement within the studied granitoids such as aplite/pegmatite dykes, veins and fractures (joints), we interpret the origin of the inter-growth texture is due to magmatic processes rather than metasomatic processes. Although acicular apatites are present in the grey granites, the absence of resorbed quartz grain boundaries, embayed crystals and quartz inclusions in mafic minerals suggest that, unlike quartz monzodiorite, the genesis of the grey granites in not related to magma mixing processes. Rather, presence of biotite mantle over amphiboles and pronounced granophyre texture along with occasional normal zoning of second generation plagioclase over the first generation crystals suggests that the grey granites are the product of equilibrium crystallization.

Similarly, absence of hornblende and presence of minor biotite in the pink granites along with the more pronounced inter-growth textures of quartz and feldspar suggest their origin from an undercooled condition. The decompression related undercooling is caused due to the rapid ascent of crystallizing magma from mid-crustal to shallow crustal levels. Presence of discrete magmatic epidotes in the studied granitoids supports this argument. Given their spatial association with quartz monzodiorite and the grey granites, the pink granites are interpreted to be formed by reworking of the quartz monzodiorites.

6.1.4. Microgeochemical evidences

As noted above, presence of mixed apatite crystal morphologies, oscillatory zoning in plagioclase, quartz with resorbed crystal boundaries and mantling of amphibole crystals over embayed quartz are all indicative of magma mixing. The P–T-f_{O2}estimates indicate that the quartz-monzodiorites were crystallized in a reducing environment at ~4.5 kbar and > 950 °C, while granites were crystallized in an oxidizing environment at < 1.5 kbar and <750 °C. The variation in the pressure suggests that the quartz-monzodiorite and granites crystallized at variable depths within mid-shallow crustal levels (< 15 km). The host TTG-gneisses and overlying upper-greenschist to lower amphibolite facies supracrustal sequences corroborates with the mid-shallow crustal depth of emplacement of quartz-monzodiorites and granites. Further, presence of pyroxene and amphibole crystals (whose P–T-f_{O2}conditions of crystallization are similar to that of quartz-monzodiorite) within low P–T granites suggests that the granitic melt is the product of the reworking of the hot crystallizing quartz-monzodiorite due to its rapid upliftment to shallow crustal levels.

6.1.5. Bulk-rock geochemical evidences

In general, the Dharwad granitoids are calc-alkaline to alkali-calcic, metaluminous and are characterized by SiO_2 (55.4–65.5 wt%) ranging between intermediate to acidic in compositions. The quartz-monzodiorites are sodic with low K_2O/Na_2O ratios (<0.5). They have higher ferromagnesian oxides (Fe_2O_3+MgO + MnO + TiO_2) (>10 wt%) as well as CaO (>5 wt%), V (306 ppm), Ni (109 ppm) and Co (31 ppm) contents. High-field strength elements [HFSE: Zr = 191 ppm, Nb = 8 ppm, Y = 23 ppm] and $_{\Sigma}$REE (112 ppm) of quartz-monzodiorite are moderate to high. The dual nature of the quartz-monzodiorite implies that it was derived from a multiple sources that involves magma mixing. However, the sodic nature of granites with high K_2O/Na_2O ratios (>0.5) as well as their relatively lower ferromagnesian oxides (<8 wt%), CaO (<3 wt%), V (<50 ppm), Ni (<1 ppm) and Co (<8 ppm) contents indicate that they are probably the differentiated products of quartz-monzodiorite. The gradual increase of HFSE (Zr = av. 472 ppm, Nb = av. 19 ppm, Y = av. 44 ppm) and ∑REE (av. 231 ppm) from quartz-monzodiorite to granites and moderately fractionated $\left[5.0 < \left(\frac{La}{Yb}\right)_N < 7.33\right]$ with no Eu anomalies in quartz-monzodiorite and marked negative Eu anomalies in granites $\left[0.7 < \left(\frac{Eu}{Eu}\right)^* < 0.85\right]$ also supports this interpretation.

Further, the overall high Al_2O_3 and CaO + Na_2O, low K and Mg# of the Dharwad granitoids does not correspond with typical high K-rich granites of the Dharwar Foreland region (Taylor et al., 1984; Mohan et al., 2014), but show characteristics of TTGs as enumerated by Laurent et al. (2014). The low Mg number (Mg#) and transitional element (Ni, Co and V) content precludes the possibility of involvement of the melt generated by direct mantle melting in the genesis of these granitoids.

6.1.6. A complex origin of the Dharwad Granitoids

Magmatic differentiation or partial melting of TTGs (Sylvester, 1994;

Davis et al., 1994; Moyen et al., 2003; Castro, 2004; Watkins et al., 2007); mixing between sanukitoid magmas and high-K leucogranite melts (Jayananda et al., 1995; Moyen et al., 2001); interaction between mantle-derived magmas and TTG continental crust (López et al., 2005; de Oliveira et al., 2009); the restite model (Chappell, 2004); partial melting of mafic lithologies (Champion and Sheraton, 1997) are some of the petrogenetic models used to explain the genesis of the Archean granitoids. Alternatively, various magma mixing models have also been proposed to explain the genesis of Archean granitoids that are characterized by similar geochemical trends as that of the studied Dharwad granitoids: mixing between a differentiated sanukitoid magma and a TTG liquid (Almeida et al., 2010); contamination of melts originating from the lower mafic crust by an older crustal component (Jayananda et al., 2006; Smithies and Champion, 2000); hybridization of TTG magmas by enriched mantle (Feng and Kerrich, 1992; Prabhakar et al., 2009); and a complex interplay of all these mechanisms (Champion and Sheraton, 1997).

The field, petrographic textural and chemical characteristics discussed above clearly illustrates the role of magma mixing in the genesis of the quartz-monzodiorites while differentiation of quartz-monzodiorite is evident in the granites. Role of melts derived from the partial melting of mantle is precluded. The dual nature of the quartz-monzodiorite (high ferromagnesian oxides and transitional elements as well as moderate to high REE-Y and HFSE contents) resembles that of melts derived from the differentiation of sanukitoids s.l. (Almeida et al., 2010; Laurent et al., 2014). Contrastingly, the high Al_2O_3 as well as low K_2O and Rb contents and low K_2O/Na_2O ratio is similar to the melts derived from the TTGs (Laurent et al., 2014). This implies that the quartz-monzodiorites were derived from the melt generated by the mixing of two melts - a melt derived from the differentiation of sanukitoids s.l. and an another melt derived from the partial melting of TTG. The partial melting of TTG perhaps took place at moderate to deeper crustal levels (~10 kbar; below plagioclase stability field) as indicated by the high CaO and the absence of Eu anomaly (Rapp et al., 1999; Martin and Moyen, 2002; Martin et al., 2005). The magma mixing probably took place at mid-crustal depths when the rapidly migrating TTG melt was intercepted by a resident magma chamber which had a pre-existing melt derived from the differentiation of sanukitoids (Fig. 13). The influx of the migrating melt into the resident magma chamber probably resulted in reducing conditions within the chamber (Fiege et al., 2017) when the quartz-monzodiorite was beginning to crystallize. As both melts had nearly the same rheological conditions, the viscosity contrasts between the two melts were low which enabled large scale mixing of the melts. Perhaps, large volumes of TTG-derived melts were injected into the resident magma chamber which favored slow cooling and mixing (Oldenburg et al., 1989; Stimac and Pearce,

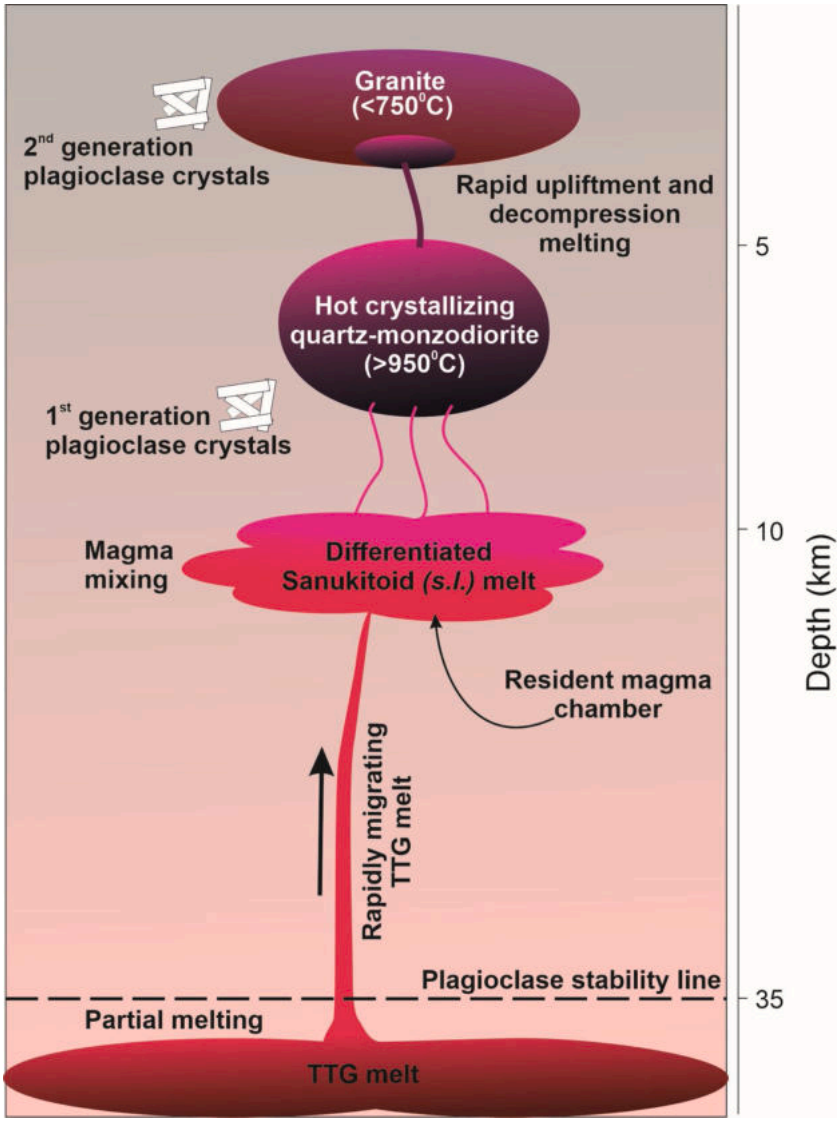

Fig. 13. Schematic conceptual cartoon illustrating the proposed origin and the magma chamber dynamics of the Dharwar granitoids.

1992). The slow cooling is also evident from the longer residual time of first generation plagioclase crystals (see below). As the mixing progressed, the crystals, that were already present in the resident magma chamber and the crystals that grew during the mixing process, were dispersed into the hybrid magma.

On the other hand, (i) field relations such as absence of sharp contact between granites and quartz-monzodiorite; (ii) petrographic evidences such as mantling of biotite over hornblende, pronounced granophyric texture, normal zoning and gradual decrease in amphiboles and slight increase in overall biotite content, significant increase of sub-solidus plagioclase with K-feldspars (perthite); (iii) microgeochemical evidences such as the general increase in albite and orthoclase from core to rim of the feldspars from quartz monzodiorites to granites; (iv) gradual decrease in pressure and temperature conditions of crystallization from quartz-monzodiorite to granites; (v) gradual increase of f_{O2}values from quartz-monzodiorites to granites; and (vi) bulk-rock geochemical characteristics such as gradual increase in SiO_2, alkalis, HFSE and REE-Y contents and gradual decrease in ferromagnesian oxides and transition element concentrations from quartz-monzodiorites to granites, suggest that the granitic melt is the product of the reworking of the hot crystallizing quartz-monzodiorite due to its rapid upliftment to shallow crustal levels. The rapid upliftment of quartz-monzodioritic magma to shallow crustal levels resulted in the decompression melting giving rise to the granitic melts (Fig. 13).

6.2. Origin of plagioclase generations and its implications on the formation of the Dharwad granitoids

The high anorthite (An) content and Fe/Al contents of the first generation plagioclase indicate the resident magma was initially granodioritic in composition. Oscillations in An composition from core (An_{47}) to rim (An_{80}) which is also manifested in oscillatory zoning and occasional sieve texture exhibited by plagioclase crystals suggest disequilibrium conditions induced into the magma chamber due to rapid changes in temperature and/or pressure (Hibbard, 1991). The rapid changes in temperature and/or pressure is interpreted to be due to an influx of hot magma into the granodioritic magma chamber. Increase in An content towards the core of first generation plagioclase crystals is possibly due to pressure fluctuations (Humphreys et al., 2006). The presence of magmatic epidotes, mixed apatite morphologies and mantling of hornblende crystals over quartz supports the fact that the changes in temperature and pressure was inevitable due to magma mixing, and these changes played an important role in the formation of the disequilibrium textures shown by the first generation plagioclase crystals.

The decrease in Fe/Al values from core to rim in the first generation plagioclase crystals suggest reducing conditions in the resident magma chamber. Significant presence of magmatic ilmenite also indicates the reducing conditions in the magma chamber. Variability in Fe or An content of plagioclase can be caused due to the increase in volatile content (Humphreys et al., 2006) or changes in melt chemistry (Kamaci and Altunkaynak, 2019). Mixing of two chemically distinct magmas is evident from the observed geochemical characteristics of the studied granitoids. Predominance of hornblende over biotite also suggests the quartz-monzodioritic magma was significantly hydrous. In light of these evidences, we interpret that the crystallization of the quartz-monzodioritic magma in a reducing environment resulted in the formation of the first generation plagioclase crystals.

Second generation plagioclase represents a new generation crystals in the evolving felsic magma chamber. The overall higher Ab contents ($Ab_{73–97}$) indicate that the second generation crystals probably originated from a hydrous magma under increased pressure. The higher oxygen fugacity values (−17.23 to −17.54) obtained for the granites indicates the role of volatile induced pressure inside the magma chamber during the crystallization of the second generation plagioclase crystals. Further, the role of pressure is also supported by the presence of two feldspars in the Dharwad granites (Luth et al., 1964; Rogers, 1988). The sharp decrease in Fe/Al in second generation plagioclase as compared to the first generation plagioclase suggests that the second generation plagioclase crystals were crystallized from a more differentiated melt after subsequent cooling.

Magma mixing is a process of physical and chemical interaction between different melts that results in disequilibrium condition. This disequilibrium directly influences the nucleation and growth rates of the crystals inside a magma chamber (Kamaci and Altunkaynak, 2019). Briefly, injection of hot magma into the relatively cooler magma chamber increases the cooling (and nucleation) rate of the resident magma (Vernon, 1984). Partial resorption of the grain boundaries and sieve and corona textures are some of the physical manifestations of disequilibrium conditions of the resident magma that are seen in the resulting crystal. As noted earlier, the CSD studies of Dharwad granitoids have shown that the magma mixing and textural coarsening have played a significant role in the origin of quartz-monzodiorite, while equilibrium crystallization and textural coarsening played a significant role during the formation of granites. The first generation plagioclase are predominant in the quartz-monzodiorite, while second generation plagioclase dominates in grey granites. The first generation crystals have a wide range of cooling temperatures as indicated by two-plagioclase thermometer. The residence time (411 yrs) of first generation crystals is almost two times greater than that of second generation plagioclase crystals (188–286 yrs). Further, the relative nucleation rate of second generation crystals (0.31–0.98) is lesser compared to the first generation crystals (Table 15). In light of all these evidences, we interpret that the resident granodioritic (which gave rise to quartz-monzodiorites) magma was formed due to magma mixing, while the grey and pink granites were generated from the low-pressure granitic melt derived from the reworking of the quartz-monzodiorite.

6.3. Model for magma chamber processes

Barometric calculations indicate that crystallization of quartz-monzodiorite occurred at relatively higher pressure (3.09–4.36 kbar) than granites (0.89–1.88 kbar). Similarly thermometric calculations using various thermometers indicate that crystallization of quartz monzodiorite occurred at higher temperatures (>950 °C) than the grey granites (<750 °C). The f_{O2}suggest that the quartz-monzodiorite crystallized in a relatively reducing environment while granites crystallized in an oxidizing environment. These data indicates that the quartz-monzodiorites and granites evolved in different magma chambers at different depths. The multistage evolution of the Dharwad granitoids is compatible with the presence of different generations of plagioclase crystals.

In stage 1, the first generation plagioclase crystallized with An rich interiors which are in near equilibrium condition. Stage 2 was marked by the influx of Ca-rich TTG-derived melts which resulted in oscillatory zoned overgrowths mantling the An-rich cores. The Ab rich rims started to mantle the An rich cores. Quartz became unstable. Resorbed and

Table 15
Plagioclase CSD results for Dharwad Granitoids.

Sample No	DG12		DG10	DG20
Rock type	Quartz Monzodiorite		Grey granite	Pink Granite
Plagioclase Generation	1	2	2	2
Slope(1/Gt)	−0.7724	−1.1085	−1.6859	−1.6086
Intercept(I/G)	−2.0189	−0.6163	−1.7398	−1.9718
Growth Rate (mm/year)	0.0031536	0.0031536	0.0031536	0.0031536
Magma Residence time	411	286	188	197
Relative nucleation rate	1	0.30526524	0.861756402	0.976670464

embayed quartz became mantled by amphiboles. In stage 3, second generation plagioclase started to crystallize in the reduced P–T environment due to decompression-driven crystallization. The abundance of second generation plagioclase crystals in the low-pressure granites further supports the decompression-driven crystallization. The uniform core to rim composition of the pyroxene crystal present in the pink granites indicate that this pyroxene crystal could be a xenocryst which escaped complete resorption due to sudden change in pressure because of decompression.

Combined petrography, mineral chemistry, CSD and bulk rock chemistry indicate that the magma mixing and subsequent decompression-driven crystallization are the principal mechanisms for the observed textural and mineralogical diversity that is characteristic of Dharwad granitoids (Fig. 13).

6.4. Crustal evolution in the northern part of the Dharwar Foreland

The Dharwar Craton, similar to almost all cratons, have witnessed three major episodes of granitoid magmatism that are related to the craton forming events at: ca. 3000 Ma, 2620–2580 Ma and 2560–2520 Ma (Chardon et al., 2011; Jayananda et al., 2018). The first two events are widespread in Foreland regions (Western Block) while the third event is restricted to Dharwar Batholith region (Eastern Block) of the Dharwar Craton. The 3000 Ma high-K plutons intrude into TTG-Sargur Group greenstone sequences whereas the ca. 2620–2580 Ma K-granites forms discrete plutons which intrude into either TTG basement or the basement-Dharwar Supergroup greenstone interface in the Foreland region (Jayananda et al., 2020, and references therein). On the other hand, the 2560–2520 Ma granitoids which marks the final stage of cratonization are regional in extent and forms major juvenile crustal accretions. They are composite plutons made up of voluminous sanukitoids, with a minor component of anatectic granites.

The high-K granitoids in the Foreland regions are generated by the reworking of an older continental crust (TTGs) with minor mantle input and these granitoids correspond to the terminal events of cratonization. The TTG emplacement in the Foreland region took place between 3600 Ma and 3320 Ma with the last phase of emplacement being at ~3200 Ma (Jayananda et al., 2020). The 3.2 Ga granodiorite intrusion perhaps marks the first stage of TTG reworking as it contains inherited zircon dated at 3.3 Ga. Followed by the last phase of TTG emplacement at 3.2 Ga, the first phase of potassic granitoid magmatism took place at 3.0 Ga (Jayananda et al., 2020) that corresponds to a major tectonothermal event at the end of TTG accretion and greenstone volcanism (Jayananda et al., 2008; Tushipokla and Jayananda, 2013; Maya et al., 2017). This 3.0 Ga K-granitoid magmatism marks the end of the juvenile crustal accretion and marks the first stage of cratonization in the Foreland region. The second stage of reworking resulted in the emplacement of c. 2.62 Ga potassic-granitoids in Arasikere-Banavara, Hosadurga and Chitradurga regions. The final stage of widespread K-magmatism of sanukitoid affinity documented in the Eastern Block (Moyen et al., 2001, 2003; Jayananda et al., 2018), however, is not yet known from the Foreland region.

Majority of the K-granitoid plutons (for e.g. Arasikere-Banavara, Hosadurga and Chitradurga) reported in literatures so far are from southern part of the Foreland region. It is to be noted that while discussing the crustal evolution process not much importance is given in the literatures to the intrusive plutons of the northern part of the Foreland region. This could be perhaps due to very few intrusive plutons reported from the northern part of the Foreland region (Gokul and Srinivasan, 1976; Dhoundial et al., 1987; Chadwick et al., 2007; Devaraju et al., 2007). However, the void created due to the lack of thorough understanding of the plutons in the north could hamper the process of reconstruction of the cratonization history in the Foreland region. For example, Dhoundial et al. (1987) reported the Rb-Sr geochronology of the trondhjemite from the Anmod Ghat region in the northwestern part of the Foreland region, which is as old as the oldest known 3.4 Ga Gorur gneiss (Beckinsale et al., 1980) in the southern part of the Foreland region. Further, it was also reported that few plutons in the northwestern part of the Foreland region belongs to 2.6 Ga widespread granite emplacement event that pervaded the craton (Dhoundial et al., 1987). This indicates that in the northern part of the Foreland region not only evidences for juvenile crustal accretion and initial stage of cratonization is preserved but they are also manifested on the surface. A detailed geochemical and geochronological studies of these granitoids could reveal a great deal about their petrogenesis, tectonothermal events, geodynamics and crustal growth process in the Foreland region.

A general attempt has been made in this study to understand the role of the intrusive plutons, occurring in the north of Foreland region, in the cratonization process. The Sm-Nd ages of the granitoids in the north of Foreland region have indicated existence of three generation plutons (Devaraju et al., 2007) - (i) the older TTG belonging to 3.3 Ga, (ii) a suite of granitoids aged between 2.96 and 2.83 Ga and (iii) the younger potassic granite belonging to 2.68 Ga. Evidences for reworking of old crust during the formation of 3.3 Ga TTG in the north has been given by Devaraju et al. (2007). Whether the juvenile crustal accretion process reported in the south of the Foreland region ended much earlier in the northern part and did the crustal reworking began much earlier in the northern part are the questions that needs further investigation.

The granitoids investigated in the present study shows clear evidences of intrusion into TTG-Dharwar Supergroup greenstone sequence. Field evidences shows that the Dharwad granitoids intrude the Upper Chitradurga Group of Dharwar Supergroup stratigraphy (Table 14) in the northern part of Shimoga greenstone belt. Further, the youngest dated rocks of the Chitradurga Group are 2.61 Ga old felsic volcanics that belongs to Lower Chitradurga Group (Table 14; Nutman et al., 1996). This 2.61 Ga felsic volcanics is overlain by ~2.6 Ga metasediments of Upper Chitradurga Group. The studied granitoids intrudes the youngest stratigraphic unit of the Chitradurga Group and are devoid of structural deformation that are conspicuous in the greenstone belt litho-units. Based on these evidences we interpret that the age of the Dharwad granitoids occurring in the north of Shimoga greenstone belt in the Foreland region could be approximately 2580−2560 Ma. Further, these granitoids marks the final stage of cratonization in the Foreland region.

7. Conclusions

An intrusive pluton into TTG-Dharwar Supergroup greenstone sequence occurring in the northern part of the Shimoga greenstone belt in the Dharwar Foreland region has been investigated in this study in order to decipher the origin and magma chamber processes of the granitoid magmas in the Foreland region. An attempt is also made to assess the crustal evolution process in the northern part of the Foreland region. Based on field and petrographic characteristics, the studied granitoids are classified as - quartz-monzodiorites and granites (grey and pink varieties). Occasional mafic bodies of dioritic-granodioritic composition with size ranging from small microgranular magmatic enclaves to bodies of several centimeters are common in these granitoids.

The granitoids are devoid of crystal-plastic fabric as well as high-strain characteristics. The textural (CSD) studies indicate that the quartz-monzodiorites are derived from magma mixing whereas the granites are derived from equilibrium crystallization of the magma derived from the reworking of quartz-monzodiorites.

The P–T estimates indicates that the quartz-monzodiorites were crystallized at higher temperature (>950 °C) and pressure (3.09–4.36 kbar) conditions in a reducing environment at mid-crustal levels. However, the granites indicate lower temperature (<750 °C) and pressure (0.89–1.88 kbar) conditions of crystallization in an oxidizing environment at shallow-crustal levels. The bulk rock chemical characteristics indicate that the quartz-monzodiorite were derived from the melt generated by the mixing of two melts - a melt derived from the differentiation of sanukitoids s.l. and a melt derived from the partial

melting of TTG. On the other hand, reworking of the hot crystallizing quartz-monzodiorite due to its rapid upliftment to shallow crustal levels resulted in a decompression melting which gave rise to granitic melts.

The relative age of the Dharwad granitoids is estimated to be ~2580–2560 Ma and unlike the other older granitoids (> 2.61 Ga) reported from the northern part of the Shimoga greenstone belt, the studied granitoids marks the final stage of cratonization in the Foreland region.

CRediT authorship contribution statement

Chandan K. Boraiaha: Conceptualization, Methodology, Visualization, Supervision, Funding acquisition, Writing - original draft, Writing - review & editing, Supervision. **Annappa G. Ugarkar:** Conceptualization, Validation, Funding acquisition, Writing - review & editing, Supervision. **Jayant K. Padhi:** Formal analysis, Resources. **Rashmi Chandan:** Formal analysis, Software. **Mallappa V. Kallapur:** Formal analysis.

Declaration of Competing Interest

The authors report no declarations of interest.

Acknowledgements

Drs. M.A. Malapur and T. Manuvachari were of great help during the field work and sample preparation. Dr. Ishwar-Kumar and Dr. Indra Sen of Indian Institute of Technology - Kanpur, Dr. G.R. Ravindra Kumar of Center for Earth Science Studies, Trivandrum and Dr. Sajeev Krishnan of Indian Institute of Science, Bengaluru are thanked for extending analytical facilities. CKB acknowledges the financial support received from Council of Scientific and Industrial Research-University Grants Commission (CSIR-UGC) in the form of Senior Research Fellowship (F.17-21/08(SA-1)). This paper forms a part of study carried out under the Department of Science and Technology (DST) funded Major Research Project (ESS/16/343/2008) to AGU. The authors are grateful to the Chairman, Department of Studies in Geology, Karnatak University, Dharwad and the Head, Department of Geology, Central University of Kerala for providing infrastructural facilities to carry out this study. The authors acknowledge the Editor-in-Chief Dr. Astrid Holzheid and the handling Editor Dr. Orhan Karsli for managing the manuscript and the two anonymous reviewers for a thorough review which helped to improve the draft version of this manuscript.

Appendix A. Supplementary data

Supplementary material related to this article can be found, in the online version, at https://doi.org/10.1016/j.chemer.2020.125688.

References

Almeida, J.d.A.C., Dall'Agnol, R., Dias, S.B., Althoff, F.J., 2010. Origin of the Archean leuco granodiorite–granite suites: evidence from the rio maria terrane and implications for granite magmatism in the Archean. Lithos 120, 235–257.
Anderson, J.L., Smith, D.R., 1995. The effects of temperature and f o2 on the al-in-hornblende barometer. Am. Mineral. 80, 549–559.
Beckinsale, R., Drury, S., Holt, R., 1980. 3,360-myr old gneisses from the south Indian craton. Nature 283, 469–470.
Boomeri, M., Nakashima, K., Lentz, D.R., 2010. The Sarcheshmeh porphyry copper deposit, Kerman, Iran: a mineralogical analysis of the igneous rocks and alteration zones including halogen element systematics related to cu mineralization processes. Ore Geol. Rev. 38, 367–381.
Boraiaha, C.K., Ugarkar, A.G., Kerr, A.C., Chandan, R., Manuvachari, T., Rajanna, S., 2018. Geology and geochemistry of metabasalts of Shimoga schist belt, Dharwar craton: implications for the late Archean basin development. Arab. J. Geosci. 11, 1–11.
Boynton, W., 1984. Geochemistry of the Rare Earth Elements: Meteorite Studies. in: Henderson.
Brandon, A.D., Creaser, R.A., Chacko, T., 1996. Constraints on rates of granitic magma transport from epidote dissolution kinetics. Science 271, 1845–1848.
Buddington, A., Lindsley, D., 1964. Iron-titanium oxide minerals and synthetic equivalents. J. Petrol. 5, 310–357.
Cashman, K.V., Marsh, B.D., 1988. Crystal size distribution (CSD) in rocks and the kinetics and dynamics of crystallization ii: Makaopuhi lava lake. Contrib. Mineral. Petrol. 99, 292–305.
Castro, A., 2004. The source of granites: inferences from the Lewisian complex. Scottish J. Geol. 40, 49–65.
Chadwick, B., Ramakrishnan, M., Viswanatha, M., 1981. Structural and metamorphic relations between Sargur and Dharwar supracrustal rocks and peninsular gneiss in central Karnataka. J. Geol. Soc. India 22, 557–569.
Chadwick, B., Vasudev, V., Jayaram, S., 1988. Stratigraphy and structure of late Archaean, Dharwar volcanic and sedimentary rocks and their basement in a part of the Shimoga basin, east of Bhadravati, Karnataka. J. Geol. Soc. India 32, 1–19.
Chadwick, B., Vasudev, V., Krishna Rao, B., Hegde, G., 1991. The stratigraphy and structure of the Dharwar supergroup adjacent to the Honnali dome: implications for late Archean basin development and regional structure in the western part of Karnataka. J. Geol. Soc. India 38.
Chadwick, B., Vasudev, V., Ahmed, N., 1996. The Sandur schist belt and its adjacent plutonic rocks implications for late Archaean crustal evolution in Karnataka. J. Geol. Soc. India 47, 37.
Chadwick, B., Vasudev, V., Hegde, G., 2000. The Dharwar craton, southern India, interpreted as the result of late Archaean oblique convergence. Precambrian Res. 99, 91–111.
Chadwick, B., Vasudev, V., Hegde, G., Nutman, A.P., 2007. Structure and shrimp u/pb zircon ages of granites adjacent to the Chitradurga schist belt: implications for Neoarchean convergence in the Dharwar craton, southern India. J. Geol. Soc. India 69, 5–24.
Chakraborti, T.M., Ray, A., Deb, G.K., 2017. Crystal size distribution analysis of plagioclase from gabbro-anorthosite suite of Kuliana, Orissa, eastern India: implications for textural coarsening in a static magma chamber. Geol. J. 52, 234–248.
Champion, D., Sheraton, J., 1997. Geochemistry and Nd isotope systematics of Archaean granites of the eastern goldfields, Yilgarn craton, Australia: implications for crustal growth processes. Precambrian Res. 83, 109–132.
Champion, D., Smithies, R., 2003. Archaean granites. In: Magmas to Mineralization: The Ishihara Symposium. Geoscience, Australia, pp. 19–24.
Chandan-Kumar, B., Ugarkar, A.G., 2017. Geochemistry of mafic-ultramafic magmatism in the western ghats belt (Kudremukh greenstone belt), western Dharwar craton, India: implications for mantle sources and geodynamic setting. Int. Geol. Rev. 59, 1507–1531.
Chappell, B., 2004. Towards a unified model for granite genesis. Earth Environ. Sci. Trans. R. Soc. Edinb. 95, 1–10.
Chardon, D., Jayananda, M., Peucat, J.J., 2011. Lateral constrictional flow of hot orogenic crust: insights from the Neoarchean of south India, geological and geophysical implications for orogenic plateaux. Geochem. Geophys. Geosystems 12.
Condie, K., 2014. Growth of continental crust: a balance between preservation and recycling. Mineral. Mag. 78, 623–638.
Cox, K., JD, B., Pankhurst, R., 1979. The Interpretation of Igneous Rocks. William Clowes, London, Britain.
Crawford, A., 1969. Reconnaissance Rb-Sr whole rock isochron studies on granitic rocks of Chitradurga and Mysore; 3. Geol. Soc. India 10, 117–166.
Davidson, J., Morgan, D., Charlier, B., Harlou, R., Hora, J., 2007. Microsampling and isotopic analysis of igneous rocks: implications for the study of magmatic systems. Annu. Rev. Earth Planet. Sci. 35, 273–311.
Davis, W., Fryers, B., King, J., 1994. Geochemistry and evolution of late Archean plutonism and its significance to the tectonic development of the slave craton. Precambrian Res. 67, 207–241.
Dawes, R.L., Evans, B.W., 1991. Mineralogy and geothermobarometry of magmatic epidote-bearing dikes, front range, Colorado. Geol. Soc. Am. Bull. 103, 1017–1031.
de Oliveira, M.A., Dall'Agnol, R., Althoff, F.J., da Silva Leite, A.A., 2009. Mesoarchean sanukitoid rocks of the Rio maria granite-greenstone terrane, Amazonian craton, brazil. J. South Am. Earth Sci. 27, 146–160.
Deb, T., Bhattacharyya, T., 2018. Interaction between felsic granitoids and mafic dykes in Bundelkhand craton: a field, petrographic and crystal size distribution study. J. Earth Syst. Sci. 127, 102.
Devaraju, T., Huhma, H., Sudhakara, T., Kaukonen, R., Alapieti, T., 2007. Petrology, geochemistry, model Sm-Nd ages and petrogenesis of the granitoids of the northern block of western Dharwar craton. J. Geol. Soc. India 70, 889.
Devaraju, T., Viljoen, R., Sawkar, R., Sudhakara, T., 2009. Mafic and ultramafic magmatism and associated mineralization in the Dharwar craton, southern India. J. Geol. Soc. India 73, 73–100.
Dhoundial, D., Paul, D., Sarkar, A., Trivedi, J., Gopalan, K., Potts, P., 1987. Geochronology and geochemistry of Precambrian granitic rocks of goa, SW India. Precambrian Res. 36, 287–302.
Dhuime, B., Hawkesworth, C.J., Delavault, H., Cawood, P.A., 2018. Rates of generation and destruction of the continental crust: implications for continental growth. Philos. Trans. Math. Phys. Eng. Sci. 376, 20170403.
Enami, M., Suzuki, K., Liou, J., Bird, D.K., 1993. Al-fe3+ and f-oh substitutions in titanite and constraints on their pt dependence. Eur. J. Mineral. 219–232.
Ernst, W., Liu, J., 1998. Experimental phase-equilibrium study of Al-and Ti-contents of calcic amphibole in MORB—a semiquantitative thermobarometer. Am. Mineral. 83, 952–969.
Feng, R., Kerrich, R., 1992. Geochemical evolution of granitoids from the Archean Abitibi southern volcanic zone and the Pontiac sub-province, superior province, Canada: implications for tectonic history and source regions. Chem. Geol. 98, 23–70.

Fiege, A., Ruprecht, P., Simon, A., 2017. A magma mixing redox trap that moderates mass transfer of sulphur and metals. Geochem. Perspect. Lett. 3, 190–199.
Frost, B.R., Frost, C.D., 2008. A geochemical classification for feldspathic igneous rocks. J. Petrol. 49, 1955–1969.
Frost, B.R., Barnes, C.G., Collins, W.J., Arculus, R.J., Ellis, D.J., Frost, C.D., 2001. A geochemical classification for granitic rocks. J. Petrol. 42, 2033–2048.
Giri, A., Anand, R., Balakrishnan, S., Dash, J., Sarma, D.S., 2019. Neoarchean magmatism in Shimoga greenstone belt, India: evidence for subduction-accretion processes in the evolution of the western Dharwar stratigraphy. Lithos 330, 177–193.
Gokul, A., Srinivasan, M., 1976. Chandranth granite. Goa. Rec. Geol. Surv. India 107, 38–45.
Harinadha Babu, P., Ponnuswamy, M., Krishnamurthy, K.V., 1981. Shimoga belt, in: early Precambrian supracrustals of southern Karnataka. Geol. Soc. India 199–218.
Hawkesworth, C.J., Dhuime, B., Pietranik, A., Cawood, P., Kemp, A.I., Storey, C., 2010. The generation and evolution of the continental crust. J. Geol. Soc. 167, 229–248.
Hawkesworth, C., Cawood, P., Dhuime, B., 2013. Continental growth and the crustal record. Tectonophysics 609, 651–660.
Helmy, H., Ahmed, A., El Mahallawi, M., Ali, S., 2004. Pressure, temperature and oxygen fugacity conditions of calc-alkaline granitoids, eastern desert of Egypt, and tectonic implications. J. Afr. Earth Sci. 38, 255–268.
Helz, R.T., 1973. Phase relations of basalts in their melting range at P_{H2O}= 5 kb as a function of oxygen fugacity: part 1 - mafic phases. J. Petrol. 14, 249–302.
Hibbard, M.J., 1991. Petrography to Petrogenesis. Prentice Hall, UK.
Higgins, M.D., 1996. Magma dynamics beneath Kameni Volcano, Thera, Greece, as revealed by crystal size and shape measurements. J. Volcanol. Geotherm. Res. 70, 37–48.
Higgins, M.D., 2000. Measurement of crystal size distributions. Am. Mineral. 85, 1105–1116.
Higgins, M.D., 2006. Quantitative Textural Measurements in Igneous and Metamorphic Petrology. Cambridge university press.
Higgins, M.D., 2011. Quantitative petrological evidence for the origin of k-feldspar megacrysts in dacites from Taapaca Volcano, Chile. Contrib. Mineral. Petrol. 162, 709–723.
Holland, T., Blundy, J., 1994. Non-ideal interactions in calcic amphiboles and their bearing on amphibole-plagioclase thermometry. Contrib. Mineral. Petrol. 116, 433–447.
Humphreys, M.C., Blundy, J.D., Sparks, R.S.J., 2006. Magma evolution and open-system processes at Shiveluch Volcano: insights from phenocryst zoning. J. Petrol. 47, 2303–2334.
Hutton, D.H., 1988. Granite emplacement mechanisms and tectonic controls: inferences from deformation studies. Earth Environ. Sci. Trans. R. Soc. Edinb. 79, 245–255.
Jayananda, M., Martin, H., Peucat, J.J., Mahabaleswar, B., 1995. Late Archaean crust-mantle interactions: geochemistry of LREE-enriched mantle derived magmas. Example of the Closepet batholith, southern India. Contrib. Mineral. Petrol. 119, 314–329.
Jayananda, M., Chardon, D., Peucat, J.J., Capdevila, R., 2006. 2.61 Ga potassic granites and crustal reworking in the western Dharwar craton, southern India: tectonic, geochronologic and geochemical constraints. Precambrian Res. 150, 1–26.
Jayananda, M., Kano, T., Peucat, J.J., Channabasappa, S., 2008. 3.35 Ga komatiite volcanism in the western Dharwar craton, southern India: constraints from Nd isotopes and whole-rock geochemistry. Precambrian Res. 162, 160–179.
Jayananda, M., Santosh, M., Aadhiseshan, K., 2018. Formation of Archean (3600–2500 ma) continental crust in the Dharwar craton, southern India. Earth. Rev. 181, 12–42.
Jayananda, M., Aadhiseshan, K., Kusiak, M.A., Wilde, S.A., Sekhamo, Ku., Guitreau, M., Santosh, M., Gireesh, R., 2020. Multi-stage crustal growth and Neoarchean geodynamics in the eastern Dharwar craton, southern India. Gondwana Res. 78, 228–260.
Jerram, D.A., Higgins, M.D., 2007. 3d analysis of rock textures: quantifying igneous microstructures. Elements 3, 239–245.
Kamaci, O., Altunkaynak, S., 2019. Magma chamber processes and dynamics beneath northwestern Anatolia: insights from mineral chemistry and crystal size distributions (csds) of the Kepsut Volcanic Complex (NW Turkey). J. Asian Earth Sci. 181, 103889.
Kerr, P.F., 1959. Optical Mineralogy. McGraw-Hill, New York.
Kumar, G.R., Sreejith, C., 2016. Petrology and geochemistry of charnockites (felsic ortho-granulites) from the Kerala Khondalite belt, southern India: evidence for intra-crustal melting, magmatic differentiation and episodic crustal growth. Lithos 262, 334–354.
Kumar, A., Rao, Y.B., Sivaraman, T., Gopalan, K., 1996. Sm-Nd ages of Archaean metavolcanics of the Dharwar craton, south India. Precambrian Res. 80, 205–216.
Larson, M., Randolph, A., 1971. Theory of Particulate Processes: Analysis and Techniques of Continuous Crystallization.
Laurent, O., Martin, H., Moyen, J.F., Doucelance, R., 2014. The diversity and evolution of late-Archean granitoids: evidence for the onset of "modern-style" plate tectonics between 3.0 and 2.5 Ga. Lithos 205, 208–235.
Leake, B.E., Woolley, A.R., Arps, C.E., Birch, W.D., Gilbert, M.C., Grice, J.D., Hawthorne, F.C., Kato, A., Kisch, H.J., Krivovichev, V.G., et al., 1997. Report. Nomenclature of amphiboles: report of the subcommittee on amphiboles of the international mineralogical association commission on new minerals and mineral names. Mineral. Mag. 61, 295–321.
Lindsley, D.H., 1983. Pyroxene thermometry. Am. Mineral. 68, 477–493.
López, S., Castro, A., García-Casco, A., 2005. Production of granodiorite melt by interaction between hydrous mafic magma and tonalitic crust. Experimental constraints and implications for the generation of Archaean TTG complexes. Lithos 79, 229–250.
Luth, W.C., Jahns, R.H., Tuttle, O.F., 1964. The granite system at pressures of 4 to 10 kilobars. J. Geophys. Res. 69, 759–773.
Marsh, B.D., 1988. Crystal size distribution (CSD) in rocks and the kinetics and dynamics of crystallization. Contrib. Mineral. Petrol. 99, 277–291. https://doi.org/10.1007/BF00375362. URL: http://link.springer.com.
Martin, H., Moyen, J.F., 2002. Secular changes in tonalite-trondhjemite-granodiorite composition as markers of the progressive cooling of earth. Geology 30, 319–322.
Martin, H., Smithies, R., Rapp, R., Moyen, J.F., Champion, D., 2005. An overview of adakite, tonalite– trondhjemite–granodiorite (TTG), and sanukitoid: relationships and some implications for crustal evolution. Lithos 79, 1–24.
Maya, J., Bhutani, R., Balakrishnan, S., Sandhya, S.R., 2017. Petrogenesis of 3.15 Ga old Banasandra komatiites from the Dharwar craton, India: implications for early mantle heterogeneity. Geosci. Front. 8, 467–481.
Mohan, M.R., Sarma, D.S., McNaughton, N.J., Fletcher, I.R., Wilde, S.A., Siddiqui, M.A., Rasmussen, B., Krapez, B., Gregory, C.J., Kamo, S.L., 2014. Shrimp zircon and titanite u-pb ages, Lu-Hf isotope signatures and geochemical constraints for 2.56 Ga granitic magmatism in western Dharwar craton, southern India: evidence for short-lived Neoarchean episodic crustal growth? Precambrian Res. 243, 197–220.
Moyen, J.F., Martin, H., Jayananda, M., 2001. Multi-element geochemical modelling of crust–mantle interactions during late-Archaean crustal growth: the Closepet granite (south India). Precambrian Res. 112, 87–105.
Moyen, J.F., Martin, H., Jayananda, M., Auvray, B., 2003. Late Archaean granites: a typology based on the Dharwar craton (India). Precambrian Res. 127, 103–123.
Naney, M., 1983. Phase equilibria of rock-forming ferromagnesian silicates in granitic systems. Am. J. Sci. 283, 993–1033.
Nutman, A., Chadwick, B., Ramakrishnan, M., Viswanatha, M., 1992. Shrimp u-pb ages of detrital zircons in Sargur supracrustal rocks in western Karnataka, southern India. J. Geol. Soc. India 39.
Nutman, A., Chadwick, B., Krishna, R., Vasudev, V., et al., 1996. Shrimp u/pb zircon ages of acid volcanic rocks in the Chitradurga and Sandur groups, and granites adjacent to the Sandur schist belt, Karnataka. J. Geol. Soc. India 47, 153–164.
Oldenburg, C.M., Spera, F.J., Yuen, D.A., Sewell, G., 1989. Dynamic mixing in magma bodies: theory, simulations, and implications. J. Geophys. Res. Solid Earth 94, 9215–9236.
Otten, M.T., 1984. The origin of brown hornblende in the Artfjället gabbro and dolerites. Contrib. Mineral. Petrol. 86, 189–199.
Peccerillo, A., Taylor, S., 1976. Geochemistry of Eocene calc-alkaline volcanic rocks from the Kastamonu area, northern turkey. Contrib. Mineral. Petrol. 58, 63–81.
Perkins, D., 1998. Mineralogy. Prentice Hall.
Peucat, J.J.J.J., Bouhallier, H., Fanning, C.M., Jayananda, M.M., 1995. Age of the Holenarsipur greenstone belt, relationships with the surrounding gneisses (Karnataka, south India). J. Geol. 103, 701–710.
Prabhakar, B., Jayananda, M., Shareef, M., Kano, T., 2009. Synplutonic mafic injections into crystallizing granite pluton from Gurgunta area, northern part of eastern Dharwar craton: implications for magma chamber processes. J. Geol. Soc. India 74, 171–188.
Putirka, K.D., 2008. Thermometers and barometers for volcanic systems. Rev. Mineral. Geochem. 69, 61–120.
Ramachandra, H., 2016. Dharwar craton-a review of regional geology and related evolutionary features. Indian J. Geosci. 70, 1–16.
Ramakrishnan, M., Vaidyanadhan, R., 2010. Geology of India (vol. 1 & 2). Geol. Soc. India Publications, Bengaluru.
Ramakrishnan, M., Venkata Dasu, S., Kroener, A., 1994. Middle Archaean age of Sargur group by single grain zircon dating and geochemical evidence for the clastic origin of metaquartzite from J.C.Pura greenstone belt, Karnataka. J. Geol. Soc. India 44, 605–616.
Rapp, R., Shimizu, N., Norman, M., Applegate, G., 1999. Reaction between slab-derived melts and peridotite in the mantle wedge: experimental constraints at 3.8 GPa. Chem. Geol. 160, 335–356.
Ridolfi, F., Renzulli, A., Puerini, M., 2010. Stability and chemical equilibrium of amphibole in Calc-alkaline magmas: an overview, new thermobarometric formulations and application to subduction related volcanoes. Contrib. Mineral. Petrol. 160, 45–66.
Rogers, J.J., 1988. The Arsikere granite of southern India: magmatism and metamorphism in a previously depleted crust. Chem. Geol. 67, 155–163.
Selby, D., Nesbitt, B.E., 2000. Chemical composition of biotite from the casino porphyry Cu-Au–Mo mineralization, Yukon, Canada: evaluation of magmatic and hydrothermal fluid chemistry. Chem. Geol. 171, 77–93.
Siahcheshm, K., Calagari, A.A., Abedini, A., Lentz, D.R., 2012. Halogen signatures of biotites from the Maher-Abad porphyry copper deposit, Iran: characterization of volatiles in syn-to post-magmatic hydrothermal fluids. Int. Geol. Rev. 54, 1353–1368.
Smithies, R., Champion, D., 2000. The Archaean high-mg diorite suite: links to tonalite–trondhjemite– granodiorite magmatism and implications for early Archaean crustal growth. J. Petrol. 41, 1653–1671.
Smithies, R.H., Champion, D.C., Van Kranendonk, M., Howard, H.M., Hickman, A.H., 2005. Modern style subduction processes in the Mesoarchean: geochemical evidence from the 3.12 Ga Whundo intra-oceanic arc. Earth Planet. Sci. Lett. 231, 221–237.
Sorcar, N., Joshi, K.B., Oliveira, E.P., Tomson, J., Nandakumar, V., 2019. Characterization of partial melting events in garnet-cordierite gneiss from the Kerala Khondalite belt, India. Geosci. Front.
Speer, J.A., 1980. Field relations and petrology of the post-metamorphic, coarse-grained granitoids and associated rocks of the southern appalachian piedmont. Proceedings Caledonides in the USA, IGCP Project 27, Caledonide Orogen, Virginia Polytechnic Institute and State University, Geological Science Memoir 2 137–148.
Srinivasan, R., Naha, K., 1993. Archaean sedimentation in the Dharwar craton, southern India. J. Earth Syst. Sci. 63, 1.

Stimac, J.A., Pearce, T.H., 1992. Textural evidence of mafic-felsic magma interaction in dacite lavas, clear lake, California. Am. Mineralogist 77, 795–809.
Streckeisen, A., 1974. Classification and nomenclature of plutonic rocks recommendations of the IUGS sub-commission on the systematics of igneous rocks. Geol. Rundschau 63, 773–786.
Sun, S., McDonough, W., 1989. Chemical and Isotopic Systematics of Oceanic Basalts: Implications for Mantle Composition and Processes. Geological Society, London, pp. 313–345. Special Publications 42.
Sylvester, P., 1994. Archaean granite plutons. In: Condie, K.C. (Ed.), Archaean Crustal Evolution.
Taylor, P., Chadwick, B., Moorbath, S., Ramakrishnan, M., Viswanatha, M., 1984. Petrography, chemistry and isotopic ages of peninsular gneiss, Dharwar acid volcanic rocks and the Chitradurga granite with special reference to the late Archean evolution of the Karnataka craton, southern India. Precambrian Res. 23, 349–375.
Trendall, A., De Laeter, J., Nelson, D., Bhaskar, R., et al., 1997a. Further zircon u-pb age data for the Daginkatte formation, Dharwar supergroup, Karnataka craton. J. Geol. Soc. India 50, 25–30.
Trendall, A., De Laeter, J., Nelson, D., Mukhopadhyay, D., 1997b. A precise zircon u-pb age for the base of the BIF of the Mulaingiri formation,(Bababudan group, Dharwar supergroup) of the Karnataka craton. J. Geol. Soc. India 50, 161–170.
Tulloch, A., 1979. Secondary ca-al silicates as low-grade alteration products of granitoid biotite. Contrib. Mineral. Petrol. 69, 105–117.
Tulloch, A., 1986. Comments and reply on "implications of magmatic epidote-bearing plutons on crustal evolution in the accreted terranes of northwestern North America" and "magmatic epidote and its petrologic significance" comment. Geology 14, 186–187.
Tushipokla, I., Jayananda, M., 2013. Geochemical constraints on komatiite volcanism from Sargur group Nagamangala greenstone belt, western Dharwar craton, southern India: implications for Mesoarchean mantle evolution and continental growth. Geosci. Front. 4, 321–340.
Ugarkar, A., Chandan Kumar, B., Manuvachari, T., 2012. Lithology and geochemistry of metavolcanics and metasediments of northern part of Dharwar-Shimoga schist belt, western dharwar craton. Indian Miner. 46, 162–178.
Ugarkar, A., Kumar, B.C., Malapur, M., Manuvachari, T., Kerr, A., 2017. Petrography and geochemistry of Archaean greywackes from northern part of the Dharwar-Shimoga greenstone belt, western Dharwar craton: implications for nature of provenance. J. Geol. Soc. India 89, 547–553.
Venkatasubramanian, V.S., Naryanaswamy, N., 1974. Rb-Sr Whole Rock Isochron Studies on Granitic Rocks From Chitradurga and North Mysore.
Vernon, R., 1984. Microgranitoid enclaves in granites—globules of hybrid magma quenched in a plutonic environment. Nature 309, 438–439.
Vernon, R.H., 2018. A Practical Guide to Rock Microstructure. Cambridge University Press.
Vincent, E., Phillips, R., 1954. Iron-titanium oxide minerals in layered gabbros of the Skaergaard intrusion, east Greenland: part i. Chemistry and ore-microscopy. Geochim. Cosmochim. Acta 6, 1–26.
Vyhnal, C.R., McSween, H.Y., Speer, J.A., 1991. Hornblende chemistry in southern Appalachian granitoids: implications for aluminum hornblende thermobarometry and magmatic epidote stability. Am. Mineral. 76, 176–188.
Watkins, J., Clemens, J., Treloar, P., 2007. Archaean TTGs as sources of younger granitic magmas: melting of sodic Metatonalites at 0.6–1.2 GPa. Contrib. Mineral. Petrol. 154, 91–110.
Whitney, J.A., Stormer, J., 1977. Two-feldspar geothermometry, geobarometry in mesozonal granitic intrusions: three examples from the piedmont of Georgia. Contrib. Mineral. Petrol. 63, 51–64.
Wones, D.R., 1989. Significance of the assemblage titanite+ magnetite+ quartz in granitic rocks. Am. Mineral. 74, 744–749.
Wyllie, P., Cox, K., Biggar, G., 1962. The habit of apatite in synthetic systems and igneous rocks. J. Petrol. 3, 238–243.
Xianwu, B., Ruizhong, H., Hanley, J., Mungall, J.E., Jiantang, P., Linbo, S., Kaixing, W., Yan, S., Hongli, L., Xiaoyan, H., 2009. Crystallization conditions (t, p, fo 2) from mineral chemistry of cu-and au-mineralised alkaline intrusions in the red river–Jinshajiang alkaline igneous belt, western Yunnan province, china. Mineral. Petrol. 96, 43.
Yavuz, F., 2007. Winamphcal: a windows program for the ima-04 amphibole classification. Geochem. Geophys. Geosystems 8.
Zen, E., Hammarstrom, J.M., 1984. Magmatic epidote and its petrologic significance. Geology 12, 515–518.
Zen, E., Hammarstrom, J., 1988. Plumbing the depth of plutons by magmatic epidote±hornblende association: a cautionary review and an example from round valley pluton, western idaho. Geological Society of America, Rocky Mountain Section Annual Meeting Abstracts 475–476.